MASTERARBEIT | MASTER'S THESIS

Titel | Title

Space-time curvature-induced corrections to Rytov's law in optical fibers

verfasst von | submitted by

Mario Michael Hudelist BSc

angestrebter akademischer Grad | in partial fulfilment of the requirements for the degree of

Master of Science (MSc)

Wien | Vienna, 2024

Studienkennzahl lt. Studienblatt | Degree programme code as it appears on the student record sheet:	UA 066 876
Studienrichtung lt. Studienblatt | Degree programme as it appears on the student record sheet:	Masterstudium Physics
Betreut von | Supervisor:	Univ.-Prof. Piotr T. Chrusciel MSc PhD
Mitbetreut von | Co-Supervisor:	Dr. Thomas Mieling BSc MSc

Abstract

The goal of this thesis is to discuss and predict space-time curvature corrections to the polarization transport of light in single-mode step-index fibers in a static space-time. According to Rytov's law, the polarization vector of light (Jones vector) follows a Fermi-Walker transport equation in optical fibers. Recent advancements in theory propose a modification to Rytov's law, which includes higher-order fiber bending corrections. To further extend the theory, a fiber is modeled in a static space-time using the ADM formalism. In this setting, a multiple-scales method is used to solve the gauge-fixed Maxwell equations for linear isotropic media, based on the assumption that the wavelength is significantly shorter than the fiber's radius of curvature, as well as the characteristic length scales of the ambient space-time. These solutions are obtained for regions of constant refractive index and have to be matched across the core-cladding interface. The resulting evolution equation for the Jones vector encodes a coupling to the spatial Riemann curvature tensor and second derivatives of the lapse function. An example is provided, where initially right circularly polarized light is predicted to acquire a small phase shift, as well as a slight perturbation indicating elliptical polarization.

Zusammenfassung

Das Ziel dieser Arbeit ist es, Raumzeitkrümmungskorrekturen zum Polarisationstransport von Licht in “single-mode” Stufenindex-Fasern, in einer statischen Raumzeit zu diskutieren, sowie Vorhersagen zu treffen. Der Polarisationsvektor des Lichtes folgt, entsprechend dem Rytovschen Gesetz, in optischen Fasern einer Fermi-Walker Transportgleichung. Im Zuge neuer wissenschaftlicher Erkenntnisse wurde Rytovs Gesetz um Faserbiegungsbeiträge ergänzt. Um weitere Ergänzungen herzuleiten, welche durch die Verallgemeinerung der Theorie von einer flachen auf eine gekrümmte Raumzeit zustande kommen, werden optische Fasern in statischen Raumzeiten mit Hilfe des ADM-Formalismus modelliert. Zu diesem Zweck werden die eichfixierten Maxwell-Gleichungen für lineare isotrope Medien, basierend auf der Annahme, dass die Wellenlänge deutlich kleiner ist als der Faserkrümmungsradius sowie die charakteristischen Längenskalen der umgebenden Raumzeit, störungstheoretisch, mittels einer “multiple-scales” Methode, gelöst. Bei Stufenindex-Fasern treten Unstetigkeiten beim Übergang zwischen Kern und Mantel auf. Daher müssen die Lösungen der Feldgleichungen an der Schnittstelle stetig sein. Dies führt zu einer Evolutionsgleichung für den Jones-Vektor. Diese Evolutionsgleichung ist charakterisiert durch eine Kopplung an den räumlichen Riemannschen Krümmungstensor, sowie an zweite Ableitungen der Lapse-Funktion. An einem Beispiel wird illustriert, wie rechtszirkular polarisiertes Licht einen kleinen Phasenschub, sowie eine Störung, welche eine leichte Eliptizität induziert, erfährt.

Contents

Chapter 1

Introduction

This thesis discusses aspects of space-time curvature-induced effects on polarized light, traveling in a cylindrical linear isotropic step-index waveguide.

1.1 Brief historic overview

The first experimental demonstration of light guidance dates back to 1841, where it was shown that light flows along a laminar stream of water in the form of a fountain [1–3]. Ten years later, Maxwell formulated a theory of electromagnetism, essentially characterizing light, which was experimentally verified by Hertz [4]. Later that century, Bell invented the "Photophone," which was able to transmit a telephone signal merely using sunlight [5]. However, the photophone failed to be commercially practical in stark contrast to his other prominent invention of the telephone [6]. One of the first documented uses of light bending in glass rods is by the Austrian medical doctor Reuss, who discussed its use to light up the eye walls [7]. In the following years, the use of optical glass fibers, specifically for imaging applications in the field of medicine, was actively researched. Shortly after the invention of the fiber cladding by A. Van Heel, the first functional prototype of an endoscope was presented by Prof. Hirschowitz to the American Gastroscopic Society in 1957 [8]. Although there are documented results on the successful transmission of television signals using glass rods already in 1933, it was not until after the invention of the laser, when, in 1966 Kao and Hockham realized that the transmission loss is mainly due to impurities in the fiberglass [1; 9]. With cladded single-mode fibers in mind, for the remarkable theoretical proposal of a possible transmission loss for telecommunication purposes below a threshold of 20 dB/km, Kao was awarded the 2009 Nobel Prize "for groundbreaking achievements concerning the transmission of light in fibers for optical communication" [10]. In 1970, Corning was able to produce the previously proposed fibers with a transmission loss below 20 dB/km thus setting the stage for the era of telecommunication [11]. The following years were marked by various theoretical and experimental achievements from the start of the operation of the first transatlantic cable up to the high-speed performance optical fibers used in modern society today.

The study of various aspects of light remains an active field of research today. The two most prominent fields of research approach the study of light from distinct perspectives. One field employs a quantum description to capture phenomena such as entanglement [12] and quantum teleportation [13], while the other utilizes a classical description to examine gravitational effects on light, including gravitational lensing [14] and gravitational redshift [15]. In experimental optics, waveguides in the form of optical fibers are typically used to investigate both quantum and gravitational effects. The GRAVITES experiment, for example, aims to measure effects at the interface of general relativity and quantum fiber optics [16]. The most comprehensive model for such experiments is currently provided by a quantum field theoretical description of fiber optics in curved space-time, as developed in [17]. In this work by Mieling, an evolution equation for the polarization vector of light is discussed, which serves as a main starting point for what follows.

1.2 Rytov's law

The key observation, around which this thesis revolves, states that the polarization of light traveling along a (space-like) path in inhomogeneous isotropic media is subject to an evolution equation [18–20]. This is one way to phrase Rytov's law, which, at its heart, aims to explain the resulting rotation of the plane of polarization. The earliest treatments of geometrical optics date back to the 16$^{\text{th}}$ century and its application for the scalar field equation was already known by Rytov [21]. His main idea was to use the geometrical optics approximation starting from Maxwell's equations. He suspected that, in contrast to the scalar wave equation, the first order reveals, in addition to the conservation of light flux, something about the polarization and its rotation [21]. Starting with an ansatz for the solutions, given in terms of the electric and the magnetic field, he aimed to solve Maxwell's equations for monochromatic waves in a dielectric. Using the geometrical optics approximation, he expanded the solution in powers of the wavelength, where the first order implied that a light ray subject to torsion experiences a rotation of the electric and magnetic field relative to the Serret-Frenet frame [22]. This rotation is described by the arc-length derivative of the angle of rotation given by

$$\frac{\mathrm{d}}{\mathrm{d}s}\phi = \tau \,, \tag{1.2.1}$$

where τ represents the torsion. The torsion is typically given in terms of the radius of torsion k according to $\tau = k^{-1}$.

The statement in Eq. (1.2.1) is mostly attributed to Rytov, however, the literature suggests, in accordance with Stigler's law[1], that E. Bortolotti derived an analogous statement using a different approach 20 years before Rytov [23]. Bortolotti essentially derived the

[1] Stigler's law of eponymy states that most works that are attributed to scientific discoveries are not named after the first inventor.

Fermi-Walker transport equation[2], which for the polarization vector of light is equivalent to Rytov's law [27]. In contrast to Rytov, Bortolotti's geometric version of Rytov's law is frame-independent.

Building up on Rytov, Vladimirksii provided the geometric interpretation of the polarization rotation in terms of an evolution of the polarization vector [19]. The equivalent geometric notion is that of a vector a following the evolution equation

$$a' - \sqrt{\gamma'' \cdot \gamma''}\,(\gamma'' \cdot a)\,\gamma' = 0\,, \tag{1.2.2}$$

where $'$ denotes the arc-length derivative and γ is the curve along which light travels. To see the equivalence, consider a decomposition of a into the Serret-Frenet frame

$$a = \cos\phi(s)N - \sin\phi(s)B\,, \tag{1.2.3}$$

where $N = \sqrt{\gamma'' \cdot \gamma''}\gamma''$ is the normalized principal normal and $B = \gamma' \times N$ is the unit bi-normal [28]. Inserting this into Eq. (1.2.2) and using the standard relations $N' = -\sqrt{\gamma'' \cdot \gamma''}\gamma' + \tau B$, as well as $B' = -\tau N$, implies

$$(-\phi' + \tau)b = 0\,, \tag{1.2.4}$$

where $b = \sin\phi(s)N + \cos\phi(s)B$. This shows the equivalence between Eq. (1.2.1) and Eq. (1.2.2). Coincidentally, in the same year, Jones invented a new calculus, later known as Jones calculus, to describe optical phenomena [29]. In this calculus, the polarization vector of light is associated with a complex vector called the Jones vector and polarization dynamics, such as the effect of a quarter-wave plate, are realized as an action of complex matrices.

In terms of this language, the main statement, referred to as Rytov's law, is as follows:

Rytov's law *The Jones vector (polarization vector) of light is Fermi-Walker transported along a curve in inhomogeneous isotropic media.*

Although some authors give direct credit to Rytov (c.f. [17; 20; 21; 30–33]), his, Bortolotti's and Vladimirskii's contributions remain largely forgotten.

1.2.1 Experimental observations

The first experimental demonstration of Rytov's law was performed by Ross, who showed that polarized light traveling through a one-turn helix with an adjustable pitch is subject to a purely geometrical rotation of linear polarization [34]. This was also verified by Tomita and Chiao using a similar experimental setup [35] and others [36; 37].

[2] The Fermi-Walker transport equation was first invented by Fermi [24] and later re-derived by Walker [25]. It provides a transport equation along a curve concerning the curve's tangent and normal direction [26].

1.2.2 Theoretical developments

The most prominent work that builds up on Rytov's law was contributed by Berry with his derivation of the Berry phase. In his work, he states, that his derivation of Rytov's law is based on Maxwell's equations [38]. However, Berry did not provide explicit calculations and postponed his derivations to another potential paper which he never published. In his work, he arrived at similar expressions as Vladimirksii. Another derivation of the Rytov law was derived by Lai, who used Maxwell's equations but did not include any boundary conditions and thus failed to deliver a suitable description of an optical fiber [39]. The most promising addition was derived by Mieling and Oancea [20]. The authors provided a derivation from the full Maxwell equations and included boundary conditions for a step-index fiber as typically used in experimental setups. Using an approximation scheme, they provided higher-order bending corrections and thus a valid extension of Rytov's law. The latest discussion on the topic can be found in a doctoral thesis by Mieling, where some possible contributions that arise from space-time curvature (i.e. from the lapse function and the shift vector field) are discussed qualitatively and hence furnish the motivation for the thesis at hand [17].

1.3 Outline

Chapter 2 of this thesis is concerned with the general geometric picture of the problem. Using a $3 + 1$ split of the space-time, the metric is approximated along a spatial curve resembling the baseline of the optical fiber, employing Fermi normal coordinates. It further discusses the description of light as a solution to Maxwell's equations in the Lorenz gauge and boundary condition for linear isotropic media with an abrupt change of refractive index on the interface.

The aim of Chapter 3 is to provide the reader with a short overview of the problem of an optical fiber in flat space-time. It introduces important notations and concepts, such as the usefulness of a complex frame, in which the field equations for the electromagnetic potential decompose, as well as a discussion of the interface conditions for a step-index fiber.

In Chapter 4, the corresponding space-time curvature corrections are derived using a multiple-scales ansatz for the electromagnetic potential. Solving the field equations order by order and matching the solutions at the interface leads to an evolution equation of the polarization vector in terms of certain space-time quantities.

Chapter 5 discusses the interpretation of the results and provides a numerical analysis of the coupling constants that appear in the evolution equation for the Jones vector as well as a short example illustrating the polarization transport along a closed loop in a post-Newtonian space-time background.

Finally, in Chapter 6, the results are compared to the literature and the difficulties that arise if the underlying space-time is dynamical are discussed, supplemented by a short treatment in Appendix A.

1.4 Conventions

Unit convention This work uses geometrized Lorentz-Heaviside units in which the vacuum permittivity μ_0, permeability ε_0 and the speed of light c are set to

$$\varepsilon_0 = \mu_0 = c = 1\,. \tag{1.4.1}$$

Einstein summation convention Various chapters feature a distinct convention regarding Greek and Latin indices and their relation to space-time or spatial indices. However, regardless of this convention, the Einstein summation convention is used throughout.

Metric signature The signature of the metric tensor g is

$$\mathrm{sign}(g) = (-,+,+,+)\,. \tag{1.4.2}$$

Chapter 2

Optical fibers in curved space-time

This chapter aims to establish the geometrical framework necessary to discuss light propagation and fiber optics within a four-dimensional curved space-time.

In Section 2.1, the space-time geometry is modeled employing a $3+1$ formalism (for a basic introduction see [40–42]), commonly utilized in numerical relativity [43], to express the metric in the ADM form (named after Arnowitt, Deser and Misner) [44].

Section 2.2 first outlines the construction of an orthonormal frame along a given curve using the Fermi-Walker transport (outlined in [45, Sec. 6.1.3]). Then, using the frame, Fermi normal coordinates (originally introduced by and named after E. Fermi [24], see [46] for a clear geometrical treatment) are constructed. Fermi normal coordinates are physically motivated by considering the baseline of an optical fiber as a curve in three-dimensional space and mathematically by the fact that, in these coordinates, the metric on the spatial slices takes on an especially simple form.

In Section 2.3, the metric is, motivated by the axial symmetry of an optical fiber, expanded in a Taylor series in the radial direction and transformed into cylindrical coordinates (following [20]). Finally, the result, expressed in terms of a complex frame, is converted into a particularly simple form.

Section 2.4 is concerned with the propagation of light in an optical fiber. Such fibers are typically regarded as linear isotropic media with a fixed refractive index in the core and the cladding, respectively. This suggests the use of (macroscopic) Maxwell equations generalized to the curved space-time background as the field equations of choice with the main quantity of interest being the electromagnetic potential (see [47] for a rigorous treatment of the generalized Maxwell equations). Working with the electromagnetic potential consequentially demands gauge fixing. This is achieved by employing a modified Lorenz gauge, involving an optical metric. The latter adapts the general space-time background to that of a medium with a refractive index. Lastly, to fit the model of a step-index fiber, matching conditions that amount to an abrupt change in refractive index on the interface between core and cladding are imposed, resulting in a total of 8 constraint equations [48].

2.1 Space-time split

Let $(\mathscr{M}, g, \nabla)$ be a four-dimensional oriented Lorentzian manifold equipped with a metric g and Levi-Civita connection ∇. The space-time $\mathscr{M}$ is assumed to be globally hyperbolic, which allows for splitting into time and space [42]. This foliation of the space-time can be achieved using a diffeomorphism ϕ such that

$$\phi : \mathscr{M} \longrightarrow \mathbf{R} \times \mathscr{N}\,, \tag{2.1.1}$$

where $(\mathscr{N}, \bar{g}, \bar{\nabla})$ is a space-like embedded three-dimensional oriented Riemannian manifold with induced Riemannian metric $\bar{g}$ and induced covariant derivative $\bar{\nabla}$. Each slice of the space-time is a space-like Cauchy hypersurface denoted by

$$\mathscr{N}_t = \{t\} \times \mathscr{N}\,, \tag{2.1.2}$$

where t is a regular scalar field on $\mathscr{M}$ with non-vanishing one-form $\mathrm{d}t \neq 0$. This means that $\mathscr{N}_t$ can be identified as the level sets for each value of t. The normal n orthogonal to $\mathscr{N}$ is the time-like co-vector field collinear to $\mathrm{d}t$ and thus is of the form

$$n = -\zeta \mathrm{d}t\,, \tag{2.1.3}$$

where ζ is called the lapse function, chosen such that $g(n, n) = -1$. Its main purpose is to relate the coordinate time of the space-time to the proper time experienced by an observer. The corresponding normal evolution co-vector field q is obtained from Eq. (2.1.3) by

$$q = \zeta n\,. \tag{2.1.4}$$

In general, the time-like foliation vector field ∂_t differs from $\sharp(q)$, where $\sharp = \flat^{-1}$ denotes the musical isomorphism map. This difference is captured by the shift vector field ξ, given as

$$\xi = \partial_t - \sharp(q)\,, \tag{2.1.5}$$

where ξ is tangential to $\mathscr{N}_t$. This implies that

$$g(\flat(\partial_t), \flat(\partial_t)) = g(\partial_t, \partial_t) = -\zeta^2 + g(\xi, \xi)\,. \tag{2.1.6}$$

Choosing local coordinates (t, x^i) on $\mathscr{M}$, where x^i are coordinates on $\mathscr{N}_t$, the metric in its ADM form reads

$$g = -(\zeta^2 - \bar{g}(\xi, \xi))\, \mathrm{d}t \otimes \mathrm{d}t + 2\xi_i\, \mathrm{d}t \otimes \mathrm{d}x^i + \bar{g}\,, \tag{2.1.7}$$

with $\zeta = \zeta(t, x^i)$ and $\xi = \xi(t, x^i)$.

In the following, the space-time $\mathscr{M}$ is considered to be stationary with some choice of a suitable foliation such that ∂_t is a Killing vector field. This means that the metric is time-independent. As a result, the quantities describing the foliation, such as the lapse function and the shift vector field depend only on spatial coordinates.

2.2 Fermi normal coordinates

The aim of this section is to provide a geometrical model of a fiber. First, the baseline of the fiber is described as a curve in space. Then, the Fermi-Walker derivative is used to construct an orthonormal frame along the entire curve. Finally, using the exponential map, Fermi normal coordinates are constructed in a tubular neighborhood of the curve.

Construction of FNC The construction of Fermi normal coordinates is based on a given curve

$$\begin{aligned} \gamma : \mathbf{R} &\longrightarrow \mathscr{N} \\ s &\longmapsto \gamma(s)\,, \end{aligned} \tag{2.2.1}$$

parametrized by arc-length s [49]. The unit vector field T tangential to γ is given by

$$T = \frac{\mathrm{d}}{\mathrm{d}s}\gamma(s)\,, \tag{2.2.2}$$

with normalization $\bar{g}(T, T) = 1$. This gives rise to the principal normal vector field denoted by N via

$$\bar{\nabla}_T T = N\,, \tag{2.2.3}$$

such that $\bar{g}(T, N) = 0$. For a fixed reference point $\gamma(0)$ it is possible to choose an orthonormal frame (T, E_x, E_y). This frame can be extended along the entire curve by imposing a transport equation. In general, a frame that is initially orthonormal at a point will fail to be orthonormal if parallel transported along the curve. To resolve this issue, it is necessary to formulate a suitable transport equation. One choice of transport for which the frame stays orthonormal with respect to the geometry of the curve is referred to as the Fermi-Walker transport equation and is defined via the Fermi-Walker derivative $\mathfrak{D}_s^{\mathrm{FW}}$ [50]. The Fermi-Walker derivative itself is defined by its action on a vector field by

$$\mathfrak{D}_s^{\mathrm{FW}} V = \bar{\nabla}_T V + \bar{g}(N, V)T - \bar{g}(T, V)N\,. \tag{2.2.4}$$

Imposing

$$\mathfrak{D}_s^{\mathrm{FW}} E_i = 0\,, \tag{2.2.5}$$

ensures the preservation of the orthogonality of the frame. Note that $\mathfrak{D}_s^{\mathrm{FW}} T = 0$ holds by construction. Hence, the frame is Fermi-Walker transported along the entire curve

$(T, E_x, E_y) = (T(s), E_x(s), E_y(s))$. The exponential map gives rise to a function

$$\psi(x^i, s) := \exp_{\gamma(s)}\{x^i E_i(s)\}\,, \tag{2.2.6}$$

which, in a neighborhood around $\gamma(s)$, erects a coordinate system $\mathscr{S} = (x^i, s)$, where on γ, the frame is identified with $(T(s), E_i(s)) = (\partial_s, \partial_i)$.

2.3 Metric expansion

In this section, the space-time metric g is Taylor expanded around a curve in the transverse directions using Fermi normal coordinates on the spatial slices.

Convention In what follows, the convention is such that space-time objects are unbarred with Greek indices corresponding to $(0, 1, 2, 3)$ while Latin indices extend over $(1, 2, 3)$, whereas on $\mathscr{N}$ objects are barred with Greek indices ranging from $(1, 2, 3)$ while Latin indices extend over $(1, 2)$. In particular, for the transverse coordinates, labelled by x^i, $(i, j, k, l) \in \{1, 2\}$ is used on $\mathscr{M}$ as well as on $\mathscr{N}$. The coordinates are chosen to be (t, x^i, s) on $\mathscr{M}$, where (x^i, s) are Fermi normal coordinates on $\mathscr{N}$.

2.3.1 Taylor expansion of the metric

Choosing coordinates $\mathscr{S}' = (t, x^i, s)$ on $\mathscr{M}$, the Taylor expansion of g along $x^i = 0$ reads

$$g_{\alpha\beta} = g_{\alpha\beta}|_{x^i=0} + \partial_k g_{\alpha\beta}|_{x^i=0}\, x^k + \frac{1}{2}\partial_k\partial_l g_{\alpha\beta}|_{x^i=0}\, x^k x^l + \mathcal{O}(x^3)\,, \tag{2.3.1}$$

where $x^i = (x^1, x^2)^T$. This yields

$$\zeta(s, x^i) = \zeta|_{x^i=0} + \partial_k \zeta|_{x^i=0}\, x^k + \frac{1}{2}\partial_k\partial_l \zeta|_{x^i=0}\, x^k x^l + \mathcal{O}(x^3)\,, \tag{2.3.2a}$$

for the lapse function, as well as

$$\xi_m(s, x^i) = \xi_m|_{x^i=0} + \partial_k \xi_m|_{x^i=0}\, x^k + \frac{1}{2}\partial_k\partial_l \xi_m|_{x^i=0}\, x^k x^l + \mathcal{O}(x^3)\,, \tag{2.3.2b}$$

for the shift, and

$$\bar{g}_{\alpha\beta} = \bar{g}_{\alpha\beta}|_{x^i=0} + \partial_k \bar{g}_{\alpha\beta}|_{x^i=0}\, x^k + \frac{1}{2}\partial_k\partial_l \bar{g}_{\alpha\beta}|_{x^i=0}\, x^k x^l + \mathcal{O}(x^3)\,, \tag{2.3.2c}$$

for the induced spatial metric. The expansion in Eq. (2.3.2) is valid for any choice of local coordinates. By employing Fermi normal coordinates, as in Section 2.2, Eq. (2.3.2c) can be worked out explicitly in terms of N and the induced Riemann curvature tensor $\bar{R}$. A detailed derivation of the metric expansion of $\bar{g}$ up to the second order in flat space can be found in [20]. To summarize the first-order results, the metric along $\gamma(s)$ reduces to the canonical form

$$\bar{g}_{\alpha\beta}|_{x^i=0} = \delta_{\alpha\beta}\,, \tag{2.3.3a}$$

with the only non-vanishing metric components to the first order given by

$$\partial_i \bar{g}_{ss}|_{x^i=0} = -2N_i \iff \bar{\Gamma}_{iss}|_{x^i=0} = -\bar{\Gamma}_{ssi}|_{x^i=0} = N_i\,. \tag{2.3.3b}$$

Eq. (2.3.3b) is derived in multiple steps. To begin with, a geodesic of the form $\gamma^\mu(\lambda) = \lambda c^\mu$, parametrized by the affine parameter λ with $c^\mu = \text{const.}$, is considered. Since γ^μ is a geodesic, it satisfies the auto-parallel equation given by

$$\bar{\nabla}_c c = 0\,. \tag{2.3.4}$$

Eq. (2.3.4), together with Eq. (2.2.5), the general formula for the Christoffel symbols of the first kind

$$\bar{\Gamma}_{\alpha\beta\gamma} = \bar{g}(\partial_\alpha, \bar{\nabla}_{\partial_\beta}\partial_\gamma)\,, \tag{2.3.5}$$

and additionally

$$\partial_i \bar{g}_{kl} = \bar{\Gamma}_{kli} + \bar{\Gamma}_{lki}\,, \tag{2.3.6}$$

leads to the result of Eq. (2.3.3b). The next order expansion can be derived from a family of geodesics $\gamma(a,\lambda)$ where a parametrizes the curves and λ is the affine parameter. To this end, consider a curve of the form

$$\gamma^\mu(a,\lambda) = \lambda(\kappa_\perp^\mu + a\eta_\perp^\mu) + a\eta_\parallel^\mu\,, \tag{2.3.7}$$

where "$\perp$" refers to the transverse directions x^i and "$\parallel$" denotes the direction along the arc length s. The corresponding velocity vector field m and displacement vector field z are given by

$$\begin{aligned} m^\mu &= \partial_\lambda \gamma^\mu|_{a=0} = \kappa_\perp^\mu\,, \\ z^\mu &= \partial_a \gamma^\mu = \lambda\eta_\perp^\mu + \eta_\parallel^\mu\,, \end{aligned} \tag{2.3.8}$$

where, w.l.o.g., m is evaluated at $a = 0$. The geodesic deviation equation or Jacobi equation reads

$$(\bar{D}_\lambda \bar{D}_\lambda z)^\mu = \bar{R}^\mu{}_{\nu\rho\delta} m^\nu z^\rho m^\delta\,. \tag{2.3.9}$$

It relates second covariant derivatives w.r.t. λ of the displacement vector field with the induced Riemann tensor $\bar{R}$. Here $\bar{D}_\lambda$ is the covariant derivative along λ defined via the chain rule. Using Eq. (2.3.8), the right-hand side yields

$$(\bar{D}_\lambda \bar{D}_\lambda z)^\mu = \bar{R}^\mu{}_{\alpha\beta\gamma} \kappa_\perp^\beta \eta_\parallel^\gamma \kappa_\perp^\alpha + \lambda \bar{R}^\mu{}_{\alpha\beta\gamma} \kappa_\perp^\beta \eta_\perp^\gamma \kappa_\perp^\alpha \,, \tag{2.3.10}$$

where, expanding the left-hand side, one finds

$$\begin{aligned}(\bar{D}_\lambda \bar{D}_\lambda z)^\mu = \bar{\Gamma}^\mu_{\alpha\beta,\gamma} m^\alpha m^\gamma \eta_\parallel^\beta + 2\bar{\Gamma}^\mu_{\alpha\beta} m^\alpha \eta_\perp^\beta + \bar{\Gamma}^\mu_{\alpha\beta} \bar{\Gamma}^\beta_{\rho\delta} m^\alpha m^\rho \eta_\parallel^\delta \\ + \lambda (\bar{\Gamma}^\mu_{\alpha\beta,\gamma} m^\alpha m^\gamma \eta_\perp^\beta + \bar{\Gamma}^\mu_{\alpha\beta} \bar{\Gamma}^\beta_{\rho\delta} m^\alpha m^\rho \eta_\perp^\delta) \,.\end{aligned} \tag{2.3.11}$$

For a full derivation of Eq. (2.3.11), see Eq. (D.1.1). Taylor expansion around $\lambda = 0 \iff x^i = 0$ and replacing all contractions with transverse vectors with Latin indices (corresponding to x^i) and all parallel contractions with the longitudinal index (corresponding to s) as well as comparing orders on the left and right-hand side gives

$$\begin{aligned}\mathcal{O}(1): \quad \bar{R}^\mu_{ijs}|_{x^i=0}\ \kappa_\perp^i \kappa_\perp^j \eta_\parallel^s = \bar{\Gamma}^\mu_{is,j}|_{x^i=0}\ \kappa_\perp^i \kappa_\perp^j \eta_\parallel^s + 2\, \underbrace{\bar{\Gamma}^\mu_{ij}|_{x^i=0}}_{=0}\ \kappa_\perp^i \eta_\perp^j \\ + (\bar{\Gamma}^\mu_{i\beta} \bar{\Gamma}^\beta_{js})|_{x^i=0}\ \kappa_\perp^i \kappa_\perp^j \eta_\parallel^s \,,\end{aligned} \tag{2.3.12a}$$

$$\begin{aligned}\mathcal{O}(\lambda): \quad \bar{R}^\mu_{ijk}|_{x^i=0}\ \kappa_\perp^i \kappa_\perp^j \eta_\perp^k = 3\bar{\Gamma}^\mu_{ik,j}|_{x^i=0}\ \kappa_\perp^i \kappa_\perp^j \eta_\perp^k + (\bar{\Gamma}^\mu_{i\beta} \underbrace{\bar{\Gamma}^\beta_{jk})|_{x^i=0}}_{=0}\ \kappa_\perp^i \kappa_\perp^j \eta_\perp^k \\ + \partial_k (\bar{\Gamma}^\mu_{i\beta} \bar{\Gamma}^\beta_{js})|_{x^i=0}\ \kappa_\perp^k \kappa_\perp^i \kappa_\perp^j \eta_\parallel^s \,.\end{aligned} \tag{2.3.12b}$$

Comparing coefficients at $\mathcal{O}(1)$ for $\mu = s$ gives

$$\begin{aligned}\bar{R}_{sijs}|_{x^i=0} &= - \underbrace{\partial_j g_{ss}|_{x^i=0}}_{-2N_j}\ \underbrace{\bar{\Gamma}_{ssi}|_{x^i=0}}_{-N_i}\ + \underbrace{g^{ss}|_{x^i=0}}_{=\delta^{ss}}\ \bar{\Gamma}_{ssi,j}|_{x^i=0}\ + \underbrace{(\bar{\Gamma}_{ssi} \bar{\Gamma}_{ssj})|_{x^i=0}}_{N_i N_j} \\ &= - N_i N_j + \bar{\Gamma}_{ssi,j}|_{x^i=0} \,.\end{aligned} \tag{2.3.13}$$

Setting $\mu = l$ at $\mathcal{O}(1)$ yields

$$\bar{R}_{lijs}|_{x^i=0} = \bar{\Gamma}^l_{is,j}|_{x^i=0} + (\bar{\Gamma}_{lis} \bar{\Gamma}_{ssj})|_{x^i=0} = \bar{\Gamma}_{lis,j}|_{x^i=0} \,. \tag{2.3.14}$$

At the next order $\mathcal{O}(\lambda)$, setting $\mu = s$, the Riemann tensor is reduced to

$$\bar{R}_{sijk}|_{x^i=0} = 3\bar{\Gamma}_{sik,j}|_{x^i=0} \,, \tag{2.3.15}$$

and further, setting $\mu = l$,

$$\bar{R}_{lijk}|_{x^i=0} = 3\bar{\Gamma}_{lik,j}|_{x^i=0} \,. \tag{2.3.16}$$

The metric can now be readily expressed in terms of the Riemann tensor. By first rewriting the second derivatives of the metric in terms of Christoffel symbols and using the previously derived relations the expanded metric is obtained as

$$\begin{aligned}\bar{g}_{\alpha\beta} = &\Big((1-N_k x^k)^2 + \bar{R}_{skls}x^k x^l\Big)\,\delta^s_\alpha \delta^s_\beta + \frac{4}{3}\bar{R}_{sklm}x^k x^l \delta^s_\alpha \delta^m_\beta \\ &+ \left(\delta_{nm} + \frac{1}{3}\bar{R}_{nklm}x^k x^l\right)\delta^n_\alpha \delta^m_\beta + \mathcal{O}(r^3)\,,\end{aligned} \tag{2.3.17}$$

or equivalently

$$\begin{aligned}\bar{g} = &\Big((1-N_k x^k)^2 + \bar{R}_{skls}x^k x^l\Big)\,\mathrm{d}s^2 + 2\left(\frac{2}{3}\bar{R}_{sklm}x^k x^l\right)\mathrm{d}s\,\mathrm{d}x^m \\ &+ \left(\delta_{ij} + \frac{1}{3}\bar{R}_{iklj}x^k x^l\right)\mathrm{d}x^i\,\mathrm{d}x^j + \mathcal{O}(r^3)\,,\end{aligned} \tag{2.3.18}$$

where $r = \sqrt{(x^1)^2 + (x^2)^2}$. This is precisely the form of the spatial metric as provided in [17].

2.3.2 Change of frame and cylindrical coordinates

In this section, the spatial dependence of the metric g, hence $\bar{g}$, is transformed into cylindrical coordinates, and all tensorial components of $\bar{g}$ will be expressed in terms of a complex frame. In the case at hand, the change of the spatial dependence is motivated by optical fibers and their axial symmetry. The complex frame, on the other hand, will be, as it will turn out, most suitable for future computations.

Complex frame The Cartesian frame E_i can be expressed in terms of a complex frame $\mathfrak{e}_\pm$ via

$$E_x = \frac{1}{\sqrt{2}}\left(\mathfrak{e}_+ + \mathfrak{e}_-\right)\,, \qquad E_y = \frac{i}{\sqrt{2}}\left(\mathfrak{e}_+ - \mathfrak{e}_-\right)\,, \tag{2.3.19}$$

The flat connection ∇_i in the transverse plane is then given by

$$\nabla_x = \frac{1}{\sqrt{2}}\left(\nabla_+ + \nabla_-\right)\,, \qquad \nabla_y = \frac{i}{\sqrt{2}}\left(\nabla_+ - \nabla_-\right)\,, \tag{2.3.20}$$

where $\nabla_\pm$ is the flat derivative in the direction of $\mathfrak{e}_\pm$. In this frame, the Taylor expansion up to the second order of any scalar function $\mathcal{T}$ in the transverse coordinates yields

$$\begin{aligned}\mathcal{T}(s,x^i) = &\mathcal{T}(s) + \frac{r}{\sqrt{2}}\Big(e^{i\vartheta}\nabla_+\mathcal{T}(s) + e^{-i\vartheta}\nabla_-\mathcal{T}(s)\Big) \\ &+ \frac{r^2}{4}\Big(e^{2i\vartheta}\nabla_+\nabla_+\mathcal{T}(s) + e^{-2i\vartheta}\nabla_-\nabla_-\mathcal{T}(s) + 2\nabla_+\nabla_-\mathcal{T}(s)\Big) + \mathcal{O}(r^3)\,,\end{aligned} \tag{2.3.21}$$

where the expansion parameters in cylindrical coordinates are $x = r\cos(\vartheta)$ and $y = r\sin(\vartheta)$. In the case of Fermi coordinates, this extends to tensor fields analogously. Since $\mathrm{d}t$ remains unchanged, Eq. (2.3.21) fully determines the tt-component expansion of the metric and hence the expansion of ζ. Using Eq. (2.3.19), $\mathcal{T}$ splits into

$$\mathcal{T}_{abc..x..def} = \frac{1}{\sqrt{2}}\left(\mathcal{T}_{abc..+..def} + \mathcal{T}_{abc..-..def}\right), \tag{2.3.22a}$$

for the x component and

$$\mathcal{T}_{abc..y..def} = \frac{i}{\sqrt{2}}\left(\mathcal{T}_{abc..+..def} - \mathcal{T}_{abc..-..def}\right), \tag{2.3.22b}$$

for the y component. Expressing the metric in cylindrical coordinates leaves $\mathrm{d}s$ unchanged and hence the only non-trivial transformations are

$$\begin{aligned} \mathrm{d}x =& \mathrm{d}(r\cos(\vartheta)) = \cos(\vartheta)\mathrm{d}r - r\sin(\vartheta)\mathrm{d}\vartheta \\ \mathrm{d}y =& \mathrm{d}(r\sin(\vartheta)) = \sin(\vartheta)\mathrm{d}r + r\cos(\vartheta)\mathrm{d}\vartheta\,. \end{aligned} \tag{2.3.23}$$

Altogether, expanding yields

$$\begin{aligned} \zeta(s,x^i) = \zeta(s) &+ \frac{r}{\sqrt{2}}\left(e^{i\vartheta}\nabla_+\zeta(s) + e^{-i\vartheta}\nabla_-\zeta(s)\right) \\ &+ \frac{r^2}{4}\left(e^{2i\vartheta}\nabla_+\nabla_+\zeta(s) + e^{-2i\vartheta}\nabla_-\nabla_-\zeta(s) + 2\nabla_+\nabla_-\zeta(s)\right) \\ &+ \mathcal{O}(r^3)\,, \end{aligned} \tag{2.3.24a}$$

for the lapse and

$$\begin{aligned} \xi_\pm(s,x^i) = \xi_\pm(s) &+ \frac{r}{\sqrt{2}}\left(e^{i\vartheta}\nabla_+\xi_\pm(s) + e^{-i\vartheta}\nabla_-\xi_\pm(s)\right) \\ &+ \frac{r^2}{4}\left(e^{2i\vartheta}\nabla_+\nabla_+\xi_\pm(s) + e^{-2i\vartheta}\nabla_-\nabla_-\xi_\pm(s) + 2\nabla_+\nabla_-\xi_\pm(s)\right) \\ &+ \mathcal{O}(r^3)\,, \end{aligned} \tag{2.3.24b}$$

for the shift, thereby defining the Taylor expansion of $g_{0\mu}$. Finally, suppressing the dependence on the arc length s, the spatial metric components are given as

$$\begin{aligned} g_{rr} =& 1\,, \\ g_{\vartheta\vartheta} =& r^2\left(1 + \frac{1}{3}r^2\bar{R}_{+-+-}\right), \\ g_{r\vartheta} =& g_{rs} = 0\,, \\ g_{s\vartheta} =& i\frac{2}{3}\sqrt{2}r^3\left(e^{-i\vartheta}\bar{R}_{+--s} + e^{i\vartheta}\bar{R}_{+-+s}\right), \\ g_{ss} =& 1 - r\sqrt{2}\left(e^{-i\vartheta}\nu_- + e^{i\vartheta}\nu_+\right) \\ &+ \frac{r^2}{2}\left(e^{-2i\vartheta}\left(\nu_-^2 - \bar{R}_{-s-s}\right) + 2\left(\nu_-\nu_+ - \bar{R}_{+s-s}\right) + e^{2i\vartheta}\left(\nu_+^2 - \bar{R}_{+s+s}\right)\right). \end{aligned} \tag{2.3.25a}$$

In the following chapters, the $\bar{R}$ notation indicating the spatial Riemann tensor will be dropped, hence $\bar{R} = R$.

2.4 Optical fibers and Maxwell field equations

The aim of this section is to discuss aspects of the optical geometry of light in fibers, following [17; 47]. In this section, Greek letters indicate space-time indices, whereas Latin letters are associated with a fixed coordinate.

2.4.1 Classical optics

The previous sections provide a suitable model to describe the geometry of optical fibers in curved space-time. Thus far, only the geometry of the fiber itself is considered. To include the description of light propagating along the fiber core, the geometric setup is supplemented by Maxwell's field equations generalized to curved space. The quantities that satisfy the macroscopic Maxwell equations are defined in the following.

Electromagnetic field strength The electromagnetic field strength tensor is the two-form F defined by

$$F = \mathrm{d}A\,, \tag{2.4.1}$$

where A is the electromagnetic potential one-form. The field strength F generalizes the electric field $\mathbf{E}$ and the magnetic field $\mathbf{B}$.

Electromagnetic excitation The $(2,0)$-tensor field denoted by G is called the electromagnetic excitation and generalizes the displacement $\mathbf{D}$ and the magnetization $\mathbf{H}$. It is, in general, non-linearly related to the field strength via constitutive equations.

Einstein-Maxwell field equations The electromagnetic field strength F and the electromagnetic excitation G satisfy the Maxwell field equations defined by

$$\begin{aligned} \mathrm{d}F = \mathrm{dd}A = 0 \\ \nabla \cdot G + j = 0\,, \end{aligned} \tag{2.4.2}$$

where j is the four current density vector field and the divergence $\nabla \cdot G = \operatorname{div} G$ is defined as the contraction of the covariant differential with the first neighboring index of G. The field equations in Eq. (2.4.2) must be supplemented by a constitutive equation that relates G and F. In vacuum, G is metrically equivalent to F, meaning

$$G^{\mu\nu} = g^{\mu\alpha} g^{\nu\beta} F_{\alpha\beta}\ , \tag{2.4.3}$$

where Latin indices refer to arbitrary space-time indices. Here the geometry of the curved space-time enters the field equation, on the one hand by the metric tensor and on the other hand via the Levi-Civita connection. The constitutive equations for linear isotropic dielectrics are presented in the following.

2.4.2 Linear isotropic media

In order to have a well-defined problem it is necessary to further specify the model. Numerous experimental setups are performed in a vacuum, hence motivating the use of Eq. (2.4.3). The main interest of the work at hand regards optical fibers. In general, a realistic model of an optical fiber includes photoelastic effects (change of optical properties of a medium through tension) giving rise to optical anisotropies and will typically be non-linear [17]. For simplification, the optical fiber is considered to be a linear isotropic dielectric. While the assumptions are not perfectly ideal, they are sufficient to understand the interplay of gravity and light in optical fibers. The field equations, in the case of linear isotropic dielectrics, become considerably simpler (see [17]).

Linear electromagnetic medium An electromagnetic medium is considered linear if the excitation G depends linearly on the field strength F. The constitutive equations in the case of linear isotropic media are of the form

$$G^{\mu\nu} = \tilde{g}^{\mu\alpha}\tilde{g}^{\nu\beta}F_{\alpha\beta}\,, \tag{2.4.4}$$

where $\tilde{g}$ denotes the optical metric [17]. The metric appearing in Eq. (2.4.4) is conformally related to Gordon's optical metric $\bar{g}$ (see [51]) via

$$\tilde{g}^{\mu\nu} = \frac{1}{\sqrt{\mu}}\bar{g}^{\mu\nu}\,, \tag{2.4.5}$$

where

$$\bar{g}^{\mu\nu} = g^{\mu\nu} + (1-n^2)v^\mu v^\nu\,. \tag{2.4.6}$$

Here, n is the refractive index related to the permittivity ϵ and the permeability μ via

$$n = \sqrt{\epsilon\mu}\,, \tag{2.4.7}$$

and v denotes the four-velocity. Since linear isotropic dielectrics are considered, it is possible to find a Lagrangian four-form $\mathscr{L}$ given by

$$\mathscr{L} = \left[-\frac{1}{4}\tilde{g}^{\mu\alpha}\tilde{g}^{\nu\beta}F_{\alpha\beta}F_{\mu\nu} + A_\mu j^\mu\right]\epsilon\,, \tag{2.4.8}$$

where ϵ is the space-time volume form, which is related to $\tilde{\epsilon}$, the volume form induced by $\tilde{g}$, by

$$\tilde{\epsilon} = \eta\epsilon\,. \tag{2.4.9}$$

Here, the relation in Eq. (2.4.9) is derived in Appendix D.2. The wave impedance

$$\eta = \sqrt{\frac{\mu}{\varepsilon}}\,, \tag{2.4.10}$$

is given in terms of the permittivity and the permeability. Note that the electromagnetic potential is determined up to gauge transformations. Therefore, introducing a gauge fixing term to Eq. (2.4.8) the gauge-modified Lagrangian four-form reads

$$\mathscr{L}_\xi = \left[-\frac{1}{4}\tilde{g}^{\mu\alpha}\tilde{g}^{\nu\beta}F_{\alpha\beta}F_{\mu\nu} - \frac{1}{2\xi}\chi^2 + A_\mu j^\mu\right]\epsilon\,, \tag{2.4.11}$$

with gauge-function

$$\chi = \frac{1}{\sqrt{\mu}}\nabla_\mu\left(\sqrt{\mu}\tilde{g}^{\mu\nu}A_\nu\right)\,, \tag{2.4.12}$$

and gauge fixing parameter ξ [17]. The gauge function expressed in terms of the optical covariant derivative is given by

$$\chi = \frac{1}{\sqrt{\epsilon}}\tilde{\nabla}_\mu\left(\sqrt{\epsilon}\tilde{g}^{\mu\nu}A_\nu\right)\,. \tag{2.4.13}$$

The equivalence of Eq. (2.4.12) and Eq. (2.4.13) is derived in Eq. (D.4.1). In general, the refractive index may be arbitrary. In the present case, only step-index fibers are considered, which have a constant refractive index in the core and in the cladding. Therefore, in regions where the permittivity and permeability are constant, the field equations resulting from the Euler-Lagrange equations

$$\tilde{\nabla}_\nu\left(G^{\nu\mu} + \frac{1}{\xi}\chi\tilde{g}^{\nu\mu}\right) + j^\mu = 0\,, \tag{2.4.14}$$

are given by

$$\tilde{\Box}A_\mu - \tilde{R}^\nu{}_\mu A_\nu - \left(1 - \frac{1}{\xi}\right)\tilde{\nabla}_\mu\chi + \tilde{g}_{\mu\nu}j^\nu = 0\,, \tag{2.4.15}$$

where $\tilde{\Box}$ and $\tilde{R}$ denote the d'Alembertian and the Ricci tensor with respect to the optical metric. In the Feynman-'t Hooft gauge ($\xi = 1$) the field equations read

$$\tilde{\Box}A_\mu - \tilde{R}^\nu{}_\mu A_\nu + \tilde{g}_{\mu\nu}j^\nu = 0\,. \tag{2.4.16}$$

In the problem at hand, there are no surface charges present, meaning $j = 0$, and therefore the gauge-fixed field equations reduce to

$$\tilde{\Box} A_\mu - \tilde{R}^\nu{}_\mu A_\nu = 0\,. \tag{2.4.17}$$

Solutions to these field equations are used to describe light in an optical fiber in a region where the permittivity and hence the refractive index (2.4.7) is constant. In a typical step-index fiber, these equations can be solved locally and thus for the core and the cladding respectively. To obtain a global solution, the jump at the interface has to be taken into account.

2.4.3 Interface conditions

In this section, the derivation of the interface conditions that arise in optical step-index fibers is discussed (see [17; 20; 48]). These encode the jumps of the electromagnetic field due to an abrupt change of refractive index in the transition region between core and cladding. In the following, coordinates are chosen such that the core-cladding interface lies at $r = 1$.

Matching conditions of step-index fibers In a cylindrical step-index fiber, the interface between the core and cladding yields a surface of discontinuity along the radial direction. These jumps are expressed as

$$[\![B]\!] := B_{\text{core}} - B_{\text{cladding}}\,, \tag{2.4.18}$$

and are hence abbreviated as $[\![B]\!]$ throughout.

In the following, these conditions at the interface are derived explicitly.

Continuity requirements To begin with, $\mathrm{d}F = 0$ implies regularity, i.e., neither containing any Dirac delta terms nor any derivatives of Dirac delta functions [52]. This implies that F is continuous and hence $\mathrm{d}A$ is continuous. For the electromagnetic field component A_μ this reduces to

$$\partial_r A_\mu + \text{continuous terms} = 0\,, \tag{2.4.19}$$

for $\mu \neq r$. Continuity of A_r is derived as follows. Neglecting any surface charges and surface currents by setting $j = 0$, the field equations read

$$\nabla_\nu G^{\nu\mu} + \tilde{g}^{\mu\nu} \nabla_\nu \chi = 0\,. \tag{2.4.20}$$

Condition	Jump
Electromagnetic potential	$[\![A_\mu]\!] = 0$
Gauge function	$[\![\chi]\!] = 0$
Electromagnetic excitation	$[\![G^{r\mu}]\!] = 0$

Table 2.1: Interface conditions for the field equations including gauge fixing [48].

These further reduce to

$$\frac{1}{\sqrt{-\det g}}\partial_r(\sqrt{-\det g}G^{r\mu}) + \tilde{g}^{r\mu}\partial_r\chi + \text{cont. terms} = 0\,, \tag{2.4.21}$$

where $\det g$, as well as $\tilde{g}^{r\mu}$, are continuous. Setting $\mu = r$, it follows that $\tilde{g}^{rr}\partial_r\chi$ is continuous and hence $[\![\chi]\!] = 0$. As an immediate consequence

$$\chi = \frac{1}{\sqrt{-\det \tilde{g}}}\partial_r\left(\sqrt{-\det \tilde{g}}\tilde{g}^{r\nu}A_\nu\right) + \text{regular terms}\,, \tag{2.4.22}$$

and since $[\![A_{\mu\neq r}]\!] = 0$ it follows

$$\chi = \tilde{g}^{rr}\partial_r A_r + \text{regular terms}\,, \tag{2.4.23}$$

which implies that $\partial_r A_r$ is regular and hence $[\![A_r]\!] = 0$. This establishes the jump condition

$$[\![A_\mu]\!] = 0\,, \tag{2.4.24}$$

for all components of the electromagnetic potential. Using the derived matching conditions from above, the regularity of the field equations implies

$$\partial_r G^{r\mu} + \text{regular terms} = 0\,. \tag{2.4.25}$$

Furthermore, since F is regular, G must be regular, as they are related via constitutive equations. Hence, $\partial_r G^{r\mu}$ is regular and as a result

$$[\![G^{r\mu}]\!] = 0\,. \tag{2.4.26}$$

The jump conditions derived in this section are compactly summarized in Table 2.1.

2.5 Summary

The geometrical setting to describe optical fibers in a four-dimensional space-time is based on the $3+1$ formalism, which introduces quantities such as the lapse function and the shift vector field. It is possible to find suitable coordinates and expand the metric in radial directions transverse to the baseline, where curvature contributions arise at the second order in the expansion parameter. Motivated by the symmetry of optical fibers, the metric is transformed to cylindrical coordinates and its components are expressed in terms of a complex frame. The final expression for the metric components is provided in Section 2.3.

Having set the geometrical stage it is necessary to incorporate field equations that govern the propagation of light in an optical step-index fiber. Introducing a modified Lorenz gauge and the optical metric $\tilde{g}$ it is possible to find a Lagrangian which (for constant refractive index n and wave impedance η) leads to a wave equation for the electromagnetic potential A given by

$$\tilde{\Box} A_\mu - \tilde{R}^\beta{}_\mu A_\beta = 0\,,$$

where the fiber is treated as a linear isotropic medium. Lastly, to account for discontinuities that arise at the interface, constraints in the form of matching conditions have to be provided. These are given by

$$[\![A_\mu]\!] = [\![\chi]\!] = [\![G^{r\mu}]\!] = 0\,,$$

where χ is the gauge function and G being the electromagnetic excitation.

Chapter 3

Optical fibers in flat space-time

The idea of this chapter is, on the one hand, to introduce important notations that will be needed in the discussion of the space-time curvature contributions and, on the other hand, to provide the reader with intuition by understanding the problem in flat space-time where an exact solution to the problem is obtainable.

The flat case is already extensively treated in the literature (see [17; 20; 53]), therefore only the most important concepts are introduced and discussed.

3.1 Ansatz and matching conditions

To begin with, consider an electromagnetic potential, where $A_\mu = A_\mu(t, r, \theta, s)$. In the flat space-time case, the metric is given in terms of the Minkowski metric. For linear-isotropic media, the optical metric is defined using the Minkowski metric in cylindrical coordinates.

Complex tetrad Decomposing the electromagnetic potential in terms of a complex tetrad

$$\mathfrak{e}_t = \partial_t \,, \qquad \mathfrak{e}_\sharp = \frac{1}{\sqrt{2}}\left(\partial_r + \frac{i}{r}\partial_\theta\right) \,, \tag{3.1.1a}$$

$$\mathfrak{e}_\parallel = \partial_s \,, \qquad \mathfrak{e}_\flat = \frac{1}{\sqrt{2}}\left(\partial_r - \frac{i}{r}\partial_\theta\right) \,, \tag{3.1.1b}$$

with associated co-tetrad

$$\mathfrak{e}^t = \mathrm{d}t \,, \qquad \mathfrak{e}^\sharp = \frac{1}{\sqrt{2}}\left(\mathrm{d}r - ir\mathrm{d}\theta\right) \,, \tag{3.1.1c}$$

$$\mathfrak{e}^\parallel = \mathrm{d}s \,, \qquad \mathfrak{e}^\flat = \frac{1}{\sqrt{2}}\left(\mathrm{d}r + ir\mathrm{d}\theta\right) \,, \tag{3.1.1d}$$

will turn out to be invaluable, as will be clear during the computation of the field equations. In the aforementioned frame, the electromagnetic potential is expressed as

$$A_\beta = A_b \, \mathfrak{e}^b{}_\beta \,, \tag{3.1.2}$$

where Greek indices are space-time indices and Latin indices are referred to as the frame indices of Eq. (3.1.1).

Ansatz for the electromagnetic potential In the pursuit of constructing monochromatic waves, the frame components of the electromagnetic potential are cast into

$$A_b = a_b(r,\theta)\, e^{i(\beta s - \omega t)}\,, \tag{3.1.3}$$

where β is the constant of propagation and ω being the angular frequency. In general, multiple modes can be excited in an optical fiber. This serves as motivation to expand the field profile $a_b(r,\theta)$ as a Fourier series

$$a_b(r,\theta) = \sum_{m\in\mathbf{Z}} a_b^{(m)}(r)\, e^{im\theta}\,, \tag{3.1.4}$$

where $a_b^{(m)}(r)$ is a radial wave profile with m being the azimuthal mode or Fourier index. To study the field equations in general, it suffices to keep the Fourier m fixed but arbitrary, hence setting

$$a_b(r,\theta) = a_b(r)\, e^{im\theta}\,. \tag{3.1.5}$$

Bessel equations Inserting Eq. (3.1.5) into the gauge-fixed field equations Eq. (2.4.17) leads to homogeneous radial Helmholtz equations, also known as Bessel equations, whose solutions are given in terms of Bessel functions [54]. For clear exposition, define the Bessel operator

$$\mathcal{B}_m = \partial_r^2 + \frac{1}{r}\partial_r - \frac{m^2}{r^2} + n^2\omega^2 - \beta^2\,, \tag{3.1.6}$$

for each mode index m respectively. Extending to frame components by

$$\underline{\mathbf{B}}_m a_b = \left(\mathcal{B}_m a_t, \mathcal{B}_m a_\parallel, \mathcal{B}_{m+1} a_\sharp, \mathcal{B}_{m-1} a_\flat\right)\,, \tag{3.1.7}$$

it is possible to express the field equations Eq. (2.4.17) in the concise form

$$\underline{\mathbf{B}}_m a_b = 0\,. \tag{3.1.8}$$

The solutions

$$a(r) = \phi_m(q,p,r) = \begin{cases} qJ_m(Ur) & r<1\,,\\ pK_m(Wr) & r>1\,,\end{cases} \tag{3.1.9}$$

are given in terms of Bessel functions J_m of the first kind within the core and modified Bessel functions of the second kind K_m outside the core, with normalized transverse wave numbers U and W. The wave numbers are related to the propagation constant β via

$$U = \sqrt{n_1^2\omega^2 - \beta^2}\,, \qquad W = \sqrt{-n_2^2\omega^2 + \beta^2}\,. \tag{3.1.10}$$

More precisely, the frame components of the solutions read

$$a_t(r) = \phi_m(q_1, p_5, r)\,, \qquad a_s(r) = \phi_m(q_2, p_6, r)\,, \tag{3.1.11a}$$

$$a_\sharp(r) = \phi_{m+1}(q_3, p_7, r)\,, \qquad a_\flat(r) = \phi_{m-1}(q_4, p_8, r)\,, \tag{3.1.11b}$$

for yet unspecified integration constants q_i and p_i, where the components are associated to different integers m. Denote by $\mathbf{q} = (q_i, p_i)^{\mathrm{T}}$ an eight-component column vector. The integer m that appears in the solutions given in Eq. (3.1.9) determines the order of the Bessel functions. To avoid confusion with the Fourier index in Eq. (3.1.5), the integer m that appears in Eq. (3.1.11) will be referred to as the "Bessel index."

Omitting dependencies, the set of solutions in Eq. (3.1.11) is compactly expressed as

$$a = \phi_m[\mathbf{q}]\,. \tag{3.1.12}$$

Jump conditions The set of solutions in Eq. (3.1.12) are local solutions for the core and the cladding respectively. To obtain a global solution, both solutions have to be matched at the interface where $r = 1$.

The interface conditions provided in Table 2.1 can be expressed in terms of an eight-component column vector $\boldsymbol{\Delta}\,[A]$ as

$$\boldsymbol{\Delta}_1\,[A] = [\![A_t]\!]\,, \tag{3.1.13a}$$

$$\boldsymbol{\Delta}_2\,[A] = [\![A_{||}]\!]\,, \tag{3.1.13b}$$

$$\boldsymbol{\Delta}_3\,[A] = [\![A_\sharp]\!]\,, \tag{3.1.13c}$$

$$\boldsymbol{\Delta}_4\,[A] = [\![A_\flat]\!]\,, \tag{3.1.13d}$$

$$\boldsymbol{\Delta}_5\,[A] = [\![\mathcal{C}^-_{+1}A_\sharp - \mathcal{C}^+_{-1}A_\flat]\!]\,, \tag{3.1.13e}$$

$$\boldsymbol{\Delta}_6\,[A] = [\![\partial_r A_{||}]\!]\,, \tag{3.1.13f}$$

$$\boldsymbol{\Delta}_7\,[A] = [\![-n^2\partial_t A_t + \tfrac{1}{\sqrt{2}}\mathcal{C}^-_{+1}A_\sharp + \tfrac{1}{\sqrt{2}}\mathcal{C}^+_{-1}A_\flat]\!]\,, \tag{3.1.13g}$$

$$\boldsymbol{\Delta}_8\,[A] = [\![n^2\{\partial_r A_t - \tfrac{1}{\sqrt{2}}\partial_t A_\sharp - \tfrac{1}{\sqrt{2}}\partial_t A_\flat\}]\!]\,, \tag{3.1.13h}$$

where the differential operator

$$\mathcal{C}^\pm_m = \partial_r \mp \frac{1}{r}\left(\frac{1}{i}\partial_\theta + m\right)\,, \tag{3.1.14}$$

is acting on the frame components of the electromagnetic potential and can be viewed as a ladder operator for the Bessel index m. The full matching condition can be reduced to the statement $\boldsymbol{\Delta}\,[A] = 0$ [17].

Therefore, inserting Eq. (3.1.12) into the matching conditions Eq. (3.1.13) leads to

$$\mathbf{\Delta}[A] = \mathbf{MNq}e^{i(\beta s + m\theta - \omega t)} = 0\,, \tag{3.1.15}$$

with complex 8×8 matrices

$$\mathbf{M} = \begin{pmatrix} 1 & 0 & 0 & 0 & -1 & 0 & 0 & 0 \\ 0 & 1 & 0 & 0 & 0 & -1 & 0 & 0 \\ 0 & 0 & -U\mathcal{G}_m^+ & 0 & 0 & 0 & W\mathcal{K}_m^+ & 0 \\ 0 & 0 & 0 & U\mathcal{G}_m^- & 0 & 0 & 0 & W\mathcal{K}_m^- \\ 0 & 0 & U & U & 0 & 0 & W & -W \\ 0 & U^2\mathcal{G}_m & 0 & 0 & 0 & -W^2\mathcal{K}_m & 0 & 0 \\ in_1^2\omega & 0 & \frac{U}{\sqrt{2}} & -\frac{U}{\sqrt{2}} & -in_2^2\omega & 0 & \frac{W}{\sqrt{2}} & \frac{W}{\sqrt{2}} \\ n_1^2U^2\mathcal{G}_m & 0 & -in_1^2\frac{\omega U}{\sqrt{2}}\mathcal{G}_m^+ & -in_1^2\frac{\omega U}{\sqrt{2}}\mathcal{G}_m^- & n_2^2W^2\mathcal{K}_m & 0 & in_2^2\frac{\omega W}{\sqrt{2}}\mathcal{K}_m^+ & in_2^2\frac{\omega W}{\sqrt{2}}\mathcal{K}_m^- \end{pmatrix}, \tag{3.1.16a}$$

and

$$\mathbf{N} = \mathrm{diag}(J_m(U), \ldots, J_m(U), K_m(W), \ldots, K_m(W))\,, \tag{3.1.16b}$$

using

$$\mathcal{G}_m(U) = \frac{J'_m(U)}{UJ_m(U)}\,, \qquad \mathcal{K}_m(W) = \frac{K'_m(W)}{WK_m(W)}\,, \tag{3.1.17a}$$

$$\mathcal{G}_m^\pm(U) = \mathcal{G}_m(U) \mp \frac{m}{U^2}\,, \qquad \mathcal{K}_m^\pm(W) = \mathcal{K}_m(W) \mp \frac{m}{W^2}\,, \tag{3.1.17b}$$

where primes denote differentiation and all dependencies are suppressed for readability [17].

Dispersion Relation In the case where the matrix **M** is non-singular, only trivial solutions are obtained. While trivial solutions are not of particular interest, a singular matrix **M** leads to a dispersion relation in terms of a vanishing determinant. The determinant of the matrix product **MN** is then factorized as

$$\det \mathbf{MN} = -\sqrt{2}\mathcal{D}_{ph}\mathcal{D}_g^2\,, \tag{3.1.18}$$

where

$$\mathcal{D}_{ph} = J_m(U)^2K_m(W)^2\left[(\mathcal{G}_m(U) + \mathcal{K}_m(W))(n_1^2\mathcal{G}_m(U) + n_2^2\mathcal{K}_m(W)) - \bar{m}^2\right]\,, \tag{3.1.19}$$

with

$$\bar{m} = \frac{m\bar{n}V^2}{U^2W^2}\,, \tag{3.1.20}$$

and

$$\mathcal{D}_{gh} = UWJ_m(U)K_m(W)\left[U^2\mathcal{G}_m(U) - W^2\mathcal{K}_m(W)\right]\,, \tag{3.1.21}$$

following the convention outlined in [17]. The factor $\bar{m}$ is expressed via the normalized frequency V, also called the V number, which itself is related to the refractive indices via

$$V = \omega\sqrt{n_1^2 - n_2^2}\,, \tag{3.1.22}$$

whereas the effective refractive index $\bar{n}$ is determined by

$$\bar{n} = \sqrt{bn_1^2 + (1-b)n_2^2}\,, \tag{3.1.23}$$

where b is known as the normalized guide index, which itself can be viewed as a conversion factor, such that

$$U = \sqrt{1-b}V\,, \qquad W = \sqrt{b}V\,, \tag{3.1.24}$$

holds [53]. The normalized guide index b is subject to the equation

$$V^2 = U^2 + W^2\,. \tag{3.1.25}$$

This ensures that it is possible to find a $b \in [0, 1]$ for which Eq. (3.1.24) is defined. The requirement that Eq. (3.1.18) vanishes means that either

$$\mathscr{D}_{ph} = 0\,, \tag{3.1.26}$$

or

$$\mathscr{D}_{gh} = 0\,. \tag{3.1.27}$$

The expressions for both quantities in Eqs. (3.1.19) and (3.1.21) depend on roots of Bessel functions and the factorization is chosen to avoid any unwanted singularities, arising from $\mathscr{J}_m$ and $\mathscr{K}_m$, and false roots. A more thorough motivation backed up by a concise derivation determining which dispersion is physical, ghost or even gauge, discussed in full detail, can be found in [48].

Physical Modes In the following, only physical modes are considered with the dispersion relation given in Eq. (3.1.26). This equation admits multiple roots for the normalized guide index b as a function of the V number. The statement that Eq. (3.1.15) must vanish implies that the solution vector $\mathbf{q}$ must lie in the kernel of $\mathbf{M}$. The kernel and co-kernel of **M** are spanned by

$$\bar{\mathbf{q}} = \begin{pmatrix} 1 \\ 0 \\ \frac{-i\sqrt{\Delta}}{\sqrt{2}}\frac{U}{V}\frac{\bar{m}-\bar{n}\mathcal{K}V^2/U^2}{\bar{m}-\bar{n}(\mathcal{J}+\mathcal{K})} \\ \frac{i\sqrt{\Delta}}{\sqrt{2}}\frac{U}{V}\frac{\bar{m}+\bar{n}\mathcal{K}V^2/U^2}{\bar{m}+\bar{n}(\mathcal{J}+\mathcal{K})} \\ 1 \\ 0 \\ \frac{-i\sqrt{\Delta}}{\sqrt{2}}\frac{W}{V}\frac{\bar{m}-\bar{n}\mathcal{K}V^2/W^2}{\bar{m}-\bar{n}(\mathcal{J}+\mathcal{K})} \\ \frac{i\sqrt{\Delta}}{\sqrt{2}}\frac{W}{V}\frac{\bar{m}+\bar{n}\mathcal{K}V^2/W^2}{\bar{m}+\bar{n}(\mathcal{J}+\mathcal{K})} \end{pmatrix}, \tag{3.1.28a}$$

and

$$(\hat{\mathbf{q}})^T = \begin{pmatrix} 1 \\ 0 \\ \frac{-i((\bar{n}V^2\mathcal{J}-\bar{m}W^2)n_1^2+(\bar{m}U^2+\bar{n}V^2\mathcal{K})n_2^2)}{\sqrt{2}(U^2\mathcal{J}+W^2\mathcal{K})(\bar{m}-\bar{n}(\mathcal{J}\mathcal{K})\omega n_1^2n_2^2)} \\ \frac{i(-n_1^4W^2\mathcal{J}+U^2\mathcal{K}n_2^4+n_1^2(\bar{m}\bar{n}V^2-(V^2\mathcal{J}+W^2(-\mathcal{J}+\mathcal{K}))n_2^2))}{\sqrt{2}(\bar{m}U^2-\bar{n}V^2\mathcal{K})(\bar{m}-\bar{n}(\mathcal{J}+\mathcal{K}))\omega n_1^2n_2^2} \\ \frac{-i(W^2\mathcal{K}n_1^2+U^2\mathcal{J}n_2^2)(\bar{m}\bar{n}-\mathcal{J}n_1^2-\mathcal{K}n_2^2)V}{\sqrt{2}(U^2\mathcal{J}+W^2\mathcal{K})(\bar{m}-\bar{n}(\mathcal{J}+\mathcal{K}))\omega n_1^2n_2^2\sqrt{W^2n_1^2-U^2n_2^2}} \\ 0 \\ \frac{i(U^2\mathcal{J}n_1^2+W^2\mathcal{K}n_2^2)}{(U^2\mathcal{J}+W^2\mathcal{K})\omega n_1^2n_2^2} \\ -\frac{V^2}{(U^2\mathcal{J}+W^2\mathcal{K})\omega^2n_1^2n_2^2} \end{pmatrix}, \tag{3.1.28b}$$

respectively. Here, $\Delta = n_1^2 - n_2^2$ is used as shorthand notation. While the use of the vector spanning the co-kernel becomes more apparent as soon as inhomogeneities arise, the vector spanning the kernel will be of immediate use as follows. **q** can be set as any vector proportional to Eq. (3.1.28a). Thus, **q** can be written as

$$\mathbf{q} = \mathcal{E}\mathbf{N}^{-1}\bar{\mathbf{q}}\,, \tag{3.1.29}$$

where $\mathcal{E}$ denotes the amplitude. This derivation is a general result for homogeneous solutions with arbitrary but fixed mode index m.

Single-mode fiber specifications Commercially available step-index fiber specifications include the effective refractive index $\bar{n}$, as provided in Eq. (3.1.23), the core radius ϱ together with the vacuum wavelength λ, and numerical aperture typically denoted by NA. Most data sheets, unfortunately, do not provide explicit information on the refractive index of the core or the cladding. However, approximate values for these parameters can be deduced from data sheet specifications provided by fiber optics companies.

As an example, consider the parameter specifications for a single-mode fiber given in

Parameter	Symbol	Value
Effective Refractive Index	$\bar{n}_1$	1.4677
	$\bar{n}_2$	1.4682
Fiber Core Radius	ϱ	$4.1\,\mu$m
Refractive Index Difference	δ	0.36 %
Wavelength	λ_1	1310 nm
	λ_2	1550 nm

Table 3.1: Specification parameters of a single-mode fiber for two different wavelengths λ_i with respective effective refractive index $\bar{n}_i$ [56].

Table 3.1. To be able to extract the refractive index for the core and cladding respectively, additional information in terms of the refractive index difference δ given by

$$\delta = \frac{n_1}{n_2} - 1\,, \tag{3.1.30}$$

is needed. This information is not provided in data sheets used at the time of this thesis (see [55]). In an older data sheet of the same company, featuring identical specifications as in Table 3.1, the refractive index difference is provided with a value of $\delta = 0.36\%$ [56].

Defining

$$n_{\text{diff}} = \delta + 1\,, \tag{3.1.31}$$

and introducing the core radius ϱ, the normalized frequency of Eq. (3.1.22) can be reexpressed as

$$V = \varrho\frac{2\pi}{\lambda}n_1\sqrt{1 - \frac{1}{n_{\text{diff}}^2}}\,. \tag{3.1.32}$$

This can be used to numerically solve the physical dispersion relation for b and the refractive indices n_i simultaneously. The results are collected in Table 3.2. Using the refractive index specifications in Table 3.2 it is possible to analyze the frequency threshold for which single-mode operation is possible. To this end, consider $\mathcal{D}_{ph} = \mathcal{D}_{ph}(V, b(V))$. Differentiation of Eq. (3.1.26) gives

$$\mathrm{d}\mathcal{D}_{ph}(V, b(V)) = \partial_V\mathcal{D}_{ph}(V, b(V))\mathrm{d}V + \partial_b\mathcal{D}_{ph}(V, b(V))\mathrm{d}b = 0\,, \tag{3.1.33}$$

which implies

$$b'(V) = -\frac{\partial_V\mathcal{D}_{ph}}{\partial_b\mathcal{D}_{ph}}\,. \tag{3.1.34}$$

For each mode index m and fixed refractive indices n_1 and n_2, one obtains various roots of Eq. (3.1.26) for a fixed maximal V number value $V_{\max} = 10$. These roots can be used

Parameter	Symbol	Value
$\lambda_1 = 1310\,\mathrm{nm}$		
Core Refractive Index	n_1	1.4701
Cladding Refractive Index	n_2	1.4659
Normalized Frequency	V_1	2.179
Normalized Guide Index	$b_1(V_1)$	0.5410
$\lambda_1 = 1550\,\mathrm{nm}$		
Core Refractive Index	n_1	1.4712
Cladding Refractive Index	n_2	1.4659
Normalized Frequency	V_2	2.069
Normalized Guide Index	$b_2(V_2)$	0.4371

Table 3.2: Numerical single-mode Fiber Parameters for $m = 1$.

to numerically solve Eq. (3.1.34) for $b \in [0, 1]$. Fig. 3.1 shows that given $n_1 = 1.4712$ and $n_2 = 1.4659$, the single-mode operation is available only for $V < 2.4$.

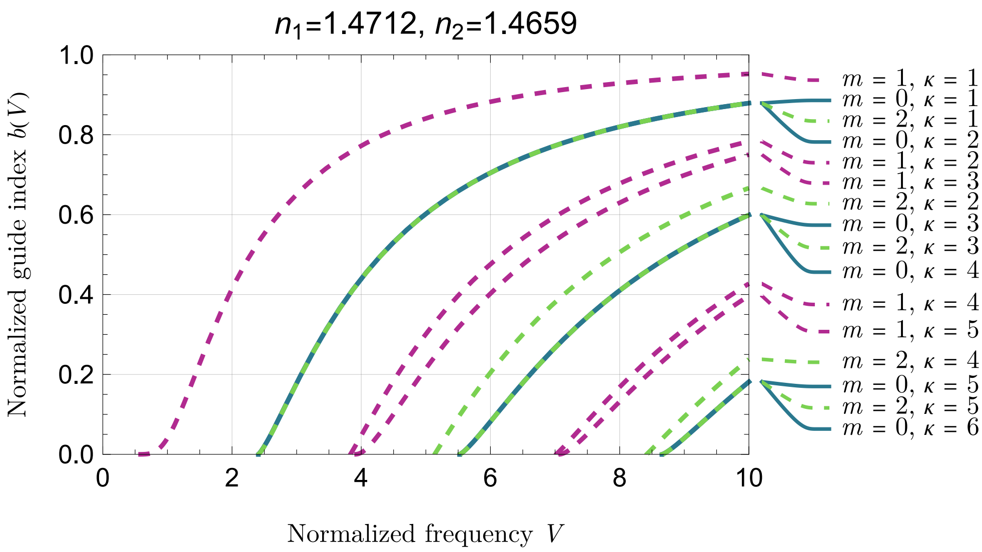

Figure 3.1: Normalized mode index $b(V)$ as a function of the normalized frequency V for different mode parameters $m \in \{0, 1, 2\}$ with corresponding roots denoted by κ.

Interpretation Working in the single-mode regime allows for an interpretation of the $\pm$ mode amplitudes as complex components of the Jones vector $\mathcal{J}$, that encodes the polarization states of light. The solution of Eq. (3.1.29) is expressed as

$$\mathbf{q}^{\pm} = \mathcal{J}^{\pm}\bar{\mathbf{q}}^{\pm}, \tag{3.1.35}$$

where $\mathcal{J}^{\pm}$ represents the $m = \pm 1$ modes. Therefore, $\mathcal{J}^{+}$ can be viewed as right circularly polarized light ($m = +1$) and $\mathcal{J}^{-}$ as left circularly polarized light ($m = -1$). Rytov's law is trivially satisfied in this case since the polarization vector is constant along the fiber's baseline.

Multi-mode regime Values above the threshold for the normalized frequency V will excite multiple modes and couplings therein. In practice, experimental setups use laser light with a typical wavelength of 1550 nm. Material properties of the fiber core limit the possible wavelength of the laser. Therefore, to operate in the multimode regime while maintaining, e.g., a wavelength of 1550 nm, it is necessary to increase the fiber core radius which directly influences the normalized frequency in accordance to Eq. (3.1.22).

In the following computations, only single-mode fibers are considered.

Chapter 4

Curvature corrections for step-index fibers

The goal of this chapter is to extend the flat space-time description of the previous chapter to that of curved space-time.

In Section 4.1 the main assumptions are outlined, which serve as motivation for a particular choice of ansatz. Further, a multiple-scales ansatz is employed.

Section 4.2 provides a detailed discussion on the order-by-order computations of the field equations including the interface conditions, where an evolution equation for the field amplitudes is obtained.

The structure of the equations and the main results are summarized in Section 4.3

The computations within this chapter are for the most part executed in Mathematica (vers. 12.3.0.0).

4.1 Ansatz and main assumptions

In order to derive corrections to Rytov's law it is necessary to impose certain restrictions on the model. The primary assumption in the computations that follow this section is that the metric coefficients have a certain characteristic length scale. This scale ultimately allows for the use of a multiple-scales method (see [57]) that is necessary to obtain solutions for the field equations in a plausible regime. The expansion coefficients in consideration are much larger than the characteristic wavelength λ_0 of an electromagnetic wave propagating through the fiber. Single-mode fibers have typical wavelengths in the order of micrometer with core radii l_0 in the same order of magnitude. Setting the core radius as a characteristic length scale turns out to be advantageous, for example when comparing distinct light beams.

Weak bending Denote by l_b the characteristic length over which a single-mode fiber is bent (typical fiber spools have a radius of curvature in the range of centimeters). This is sufficiently larger than the core radius of a fiber l_0. Under the weak bending assumption, an arbitrary fiber quantity κ with dimension $[\kappa] = (\text{length})^p$ takes the general form

$$\kappa(s) = l_b^p \tilde{\kappa}\left(\frac{\varepsilon s}{l_0}\right), \tag{4.1.1}$$

where $\tilde{\kappa}$ is a dimensionless function, with derivatives having the same order of magnitude as $\tilde{\kappa}$ itself, with dimensional scale parameter $\varepsilon = \frac{l_0}{l_b}$ and s is the arc length of the fiber baseline [17]. The scale parameter ε is thus typically in the order of 10^{-4} and hence $\varepsilon \ll 1$. Further, the expansion coefficients of the metric are exceedingly larger than the optical wavelength λ_0, since the core radius is on the same order of magnitude as the characteristic wavelength $l_0 \approx \lambda_0$. Besides general quantities, as in Eq. (4.1.1), the most prominent quantities in this work are the Riemann curvature tensor and the lapse function. Both quantities are assumed to be slowly varying along the fiber.

Riemann curvature tensor The relation of the slowly varying spatial Riemann curvature tensor $R = R(s)$, along the baseline of the fiber, with the scale parameter ε is given by

$$l_0^2 R_{abcd}(s) = \varepsilon^2 \tilde{R}_{abcd}\left(\frac{\varepsilon s}{l_0}\right). \tag{4.1.2}$$

A motivation for the form of Eq. (4.1.2) and its relation to the slowness ε is given in Appendix D.

Lapse function The other important quantity that appears in the metric is the lapse function from Eq. (2.3.24a), which in the present case is slowly varying

$$\zeta(s) = \tilde{\zeta}\left(\frac{\varepsilon s}{l_0}\right). \tag{4.1.3}$$

However, only the zeroth and second order in the expansion of the lapse will be taken into account. The reason for this choice is to simplify the problem where only terms in $\mathcal{O}(1)$ and $\mathcal{O}(\varepsilon^2)$ are considered. This is motivated by the appearance of the Fourier index m (associated with the azimuthal angle θ) in the expansion given in Eq. (2.3.24a). The characterization of quantities, such as the lapse function and the spatial Riemann curvature tensor, in terms of the corresponding Fourier index, is provided in Table 4.1.

Shift vector field The assumption that the space-time is static allows for a vanishing shift vector field. Therefore, to avoid this additional layer of complexity, the shift vector field is set to zero throughout the upcoming computation.

For simplification, the core radius is set to $l_0 = 1$. Further, the tilde notation for dimensionless quantities will be dropped whenever there can be no confusion due to the

Term	Radial index (r)	Mode index (m)
ζ	0	0
$\nabla_\pm \nabla_\pm \zeta$	2	± 2
$R_{\|+\|-}$	2	0
R_{+-+-}	2	0
$R_{\|\pm+-}$	2	± 1
$R_{\|\pm\|\pm}$	2	± 2

Table 4.1: Classification of metric coefficients in terms of their radial and angular dependence.

dependence on the expansion parameter. Hence, one has $\tilde{\kappa}(\varepsilon s) = \kappa(\varepsilon s)$.

Space-time corrections To keep the main focus on the space-time curvature correction and therefore extend the current literature from flat to curved space-time, only the space-time corrections will be considered. This means that all higher-order bending corrections, as derived in [18], will be neglected.

Step-index fiber Lastly, a (realistic) model of a single-mode step-index fiber is considered. To this end, the fiber's cross-section is assumed to be circular. Specializing the problem to a step-index fiber, the core refractive index n_1 is assumed to be larger than the refractive index of the cladding n_2, hence $n_1 > n_2 \geq 1$. This ensures that light is guided within the fiber.

To operate in the single-mode regime, where $l_0 \approx \lambda_0$, the normalized frequency, denoted by V, needs to stay below the threshold of $V < 2.4$. This is satisfied in typical single-mode step-index fibers. The motivation behind this is provided in the following chapter.

Mode couplings The ansatz for the electromagnetic potential features a Fourier series decomposition in the angular variable θ over the Fourier index m. This gives rise to mode-dependent perturbations, which in turn result in off-resonant and resonant couplings of the Fourier modes [17]. In simplified terms, off-resonant perturbations are mainly related to amplitude dynamics, while resonant perturbations induce phase shifts. The computations in the following chapter are, for the most part, devoted to resonant perturbations and therefore resonant mode couplings. Modes with resonant coupling $m = \pm 1$ ($e^{\pm i\theta}$) arise at second order in the perturbation and effectively couple to the nearest neighbor, whereas $m = \pm 2$ ($e^{\pm 2i\theta}$) admits a resonant coupling already at first order. Terms with Fourier index $m = 0$ give rise to phase perturbations while $m \neq 0$ terms introduce perturbations of the electromagnetic polarization, which will, in the following, be related to spatial Riemann curvature tensor terms, as well as second derivatives of the lapse function, given in Table 4.1.

A full treatment on the classification of terms that describe space-time-related fiber dynamics can be found in [17].

Ansatz for the electromagnetic potential In the pursuit of constructing monochromatic waves, the frame components (given in terms of the complex tetrad in Section 3.1), of the electromagnetic potential A are cast into

$$A_b = a_b(r, \varsigma, \theta)\, e^{i(\psi(s)-\omega t)}\,, \tag{4.1.4}$$

with optical phase given by

$$\psi(s) = \int_0^s \beta(\varepsilon s')\mathrm{d}s'\,, \tag{4.1.5}$$

where $\beta(\varsigma)$ is the modulated "constant" of propagation, which is now slowly varying, and ω is the angular frequency. Motivated by the form of the fiber modes and their couplings, the field $a_b(r, \varsigma, \theta)$ is expanded as a Fourier series

$$a_b(r, \varsigma, \theta) = \sum_{m\in\mathbf{Z}} a_b^{(m)}(r, \varsigma)\, e^{im\theta}\,, \tag{4.1.6}$$

where $a_b^{(m)}(r, \varsigma)$ is the slowly varying radial wave profile, depending on the long distance-scale ς and m is the Fourier mode index.

Multiple-scales ansatz In the regime where $\varepsilon \ll 1$, the aforementioned quantities, which enter the metric, have length scales that are significantly larger than the characteristic wavelength or, equivalently, the core radius. This requirement allows for the use of a multiple-scales expansion, which in turn is necessary to solve the field equations. A short example discussing the multiple-scales method for two coupled oscillators is provided in Appendix B.

Introducing the slowly varying scale ς, the expansion of the field $a_b(r, \varsigma, \theta)$, up to second order in the slowness parameter $\varepsilon = \varsigma/s$, is given by

$$a_b(r, \varsigma, \theta) = \sum_{m=\pm1} \left[a_b^{(0,m)}(r, \varsigma) + \varepsilon\, a_b^{(1,m)}(r, \varsigma)\right]\, e^{im\theta} \tag{4.1.7}$$

$$+ \sum_{m=-3}^{+3} \varepsilon^2\, a_b^{(2,m)}(r, \varsigma)\, e^{im\theta}\,, \tag{4.1.8}$$

where $m \in \mathbf{Z}$. The different intervals are motivated by the classification of terms in Table 4.1, where on the one hand, the space-time curvature-related terms are expected to appear only at second order in the expansion parameter and on the other hand, terms in $\mathcal{O}(\varepsilon^2)$ induce couplings between different Fourier mode indices m.

Interface conditions The jump conditions from Eq. (3.1.13) remain for the most part unchanged, with one exception being

$$\mathbf{\Delta}_7\,[A] = [\![-n^2\zeta^{-2}\partial_t A_t + \tfrac{1}{\sqrt{2}}\mathcal{C}^-_{+1}A_\sharp + \tfrac{1}{\sqrt{2}}\mathcal{C}^+_{-1}A_\flat]\!]\,, \tag{4.1.9}$$

where the lapse enters via the time component of the metric.

4.2 Solving the field equations

In the following, the field equations are solved using the multiple-scales ansatz from the previous section.

Dependencies In contrast to the flat-space case, many quantities are now slowly varying, many of which do not directly depend on ς, but rather indirectly via the lapse function $\zeta = \zeta(\varsigma)$.

- Modulated propagation constant $\beta = \beta(\varsigma)$
- Modulated lapse function $\zeta = \zeta(\varsigma)$

Field equations at $\mathcal{O}(\varepsilon^0)$ In the unperturbed case, as discussed in the previous chapter, the field equations reduce to homogeneous Bessel equations

$$\underline{\mathbf{B}}_m a_b^{(0,m)} = 0\,, \tag{4.2.1}$$

where the underlying Bessel operator is now given by

$$\mathcal{B}_m = \partial_r^2 + \frac{1}{r}\partial_r - \frac{m^2}{r^2} + \frac{n^2\omega^2}{\zeta(\varsigma)^2} - \beta^2(\varsigma)\,. \tag{4.2.2}$$

The solution in this case depends on the slow-scale ς and reads

$$a^{(0,m)}(\varsigma, r) = f_m(q(\varsigma), p(\varsigma), r) = \begin{cases} q(\varsigma)J_m(U(\varsigma)r) & r < 1\,, \\ p(\varsigma)K_m(W(\varsigma)r) & r > 1\,, \end{cases} \tag{4.2.3}$$

with modulated wave numbers

$$U = \sqrt{\frac{n_1^2\omega^2}{\zeta(\varsigma)^2} - \beta(\varsigma)^2}\,, \tag{4.2.4}$$

and

$$W = \sqrt{-\frac{n_2^2\omega^2}{\zeta(\varsigma)^2} + \beta(\varsigma)^2}\,. \tag{4.2.5}$$

The modulated frame components of the solutions read

$$a_t^{(0,m)}(\varsigma, r) = f_m(q_1(\varsigma), p_5(\varsigma), r)\,, \qquad a_s^{(0,m)}(\varsigma, r) = f_m(q_2(\varsigma), p_6(\varsigma), r)\,, \tag{4.2.6a}$$

$$a_\sharp^{(0,m)}(\varsigma, r) = f_{m+1}(q_3(\varsigma), p_7(\varsigma), r)\,, \qquad a_\flat^{(0,m)}(\varsigma, r) = f_{m-1}(q_4(\varsigma), p_8(\varsigma), r)\,, \tag{4.2.6b}$$

with integration coefficients $q_i(\varsigma)$ and $p_i(\varsigma)$. As in the flat space example, one defines a coefficient vector $\mathbf{q}^{(0)}$ such that

$$a^{(0,m)} = f_m[\mathbf{q}^{(0)}]\,, \tag{4.2.7}$$

where dependencies are suppressed for readability.

Jump conditions at $\mathcal{O}(\varepsilon^0)$ In order to obtain a global solution, the core and cladding solutions have to be matched at the interface where $r = 1$, in full analogy to the flat space case. The interface conditions are given by

$$\mathbf{\Delta}[A]/e^{i(\psi(s)+m\theta-\omega t)} = \mathbf{M^0 N q^{(0)}} + \mathcal{O}(\varepsilon) = 0\,, \tag{4.2.8}$$

where

$$\mathbf{M^0} = \begin{pmatrix} 1 & 0 & 0 & 0 & -1 & 0 & 0 & 0 \\ 0 & 1 & 0 & 0 & 0 & -1 & 0 & 0 \\ 0 & 0 & -U\mathcal{J}_m^+ & 0 & 0 & 0 & W\mathcal{K}_m^+ & 0 \\ 0 & 0 & 0 & U\mathcal{J}_m^- & 0 & 0 & 0 & W\mathcal{K}_m^- \\ 0 & 0 & U & U & 0 & 0 & W & -W \\ 0 & U^2\mathcal{J}_m & 0 & 0 & 0 & -W^2\mathcal{K}_m & 0 & 0 \\ in_1^2\zeta^{-2}\omega & 0 & \frac{U}{\sqrt{2}} & -\frac{U}{\sqrt{2}} & -in_2^2\zeta^{-2}\omega & 0 & \frac{W}{\sqrt{2}} & \frac{W}{\sqrt{2}} \\ n_1^2U^2\mathcal{J}_m & 0 & -in_1^2\frac{\omega U}{\sqrt{2}}\mathcal{J}_m^+ & -in_1^2\frac{\omega U}{\sqrt{2}}\mathcal{J}_m^- & n_2^2W^2\mathcal{K}_m & 0 & in_2^2\frac{\omega W}{\sqrt{2}}\mathcal{K}_m^+ & in_2^2\frac{\omega W}{\sqrt{2}}\mathcal{K}_m^- \end{pmatrix}, \tag{4.2.9a}$$

now depends on the lapse function but remains largely the same as in the flat space-time case. Note that for simplicity equation Eq. (4.2.8) is discussed for a fixed azimuthal mode index m but in general features a linear combination of the modes. The statement that Eq. (4.2.8) holds implies that the solution vector $\mathbf{q}^{(0)}$, which is now slowly varying, must lie in the kernel of $\mathbf{M^0}$. The kernel of the matrix $\mathbf{M^0}$ is spanned by

$$\bar{\mathbf{q}}^{(0)} = \begin{pmatrix} \zeta \\ 0 \\ \frac{-i\sqrt{\Delta}}{\sqrt{2}}\frac{U}{V}\frac{\bar{m}-\bar{n}\mathcal{K}V^2/U^2}{\bar{m}-\bar{n}(\mathcal{J}+\mathcal{K})} \\ \frac{i\sqrt{\Delta}}{\sqrt{2}}\frac{U}{V}\frac{\bar{m}+\bar{n}\mathcal{K}V^2/U^2}{\bar{m}+\bar{n}(\mathcal{J}+\mathcal{K})} \\ \zeta \\ 0 \\ \frac{-i\sqrt{\Delta}}{\sqrt{2}}\frac{W}{V}\frac{\bar{m}-\bar{n}\mathcal{K}V^2/W^2}{\bar{m}-\bar{n}(\mathcal{J}+\mathcal{K})} \\ \frac{i\sqrt{\Delta}}{\sqrt{2}}\frac{W}{V}\frac{\bar{m}+\bar{n}\mathcal{K}V^2/W^2}{\bar{m}+\bar{n}(\mathcal{J}+\mathcal{K})} \end{pmatrix} . \tag{4.2.10}$$

Thus, the solution vector $\mathbf{q}^{(0)}$ can be written as

$$\mathbf{q}^{(0)} = \mathcal{E}^{(0)}(\varsigma)\bar{\mathbf{q}}^{(0)}(\varsigma)\,, \tag{4.2.11}$$

where $\mathcal{E}^{(0)}(\varsigma)$ is an amplitude that slowly varies along the long distance-scale ς. Note that this derivation is a general result for the homogeneous solutions with arbitrary but fixed mode index m. Since the unperturbed case only admits $m = \pm 1$ modes the $\mathcal{O}(\varepsilon^0)$ result is given in terms of

$$\mathbf{q}^{(0,\pm 1)} = \mathcal{E}^{(0)}_{\pm}(\varsigma)\bar{\mathbf{q}}^{(0)}_{\pm}\,, \tag{4.2.12}$$

indicating the respective mode solutions whose amplitudes are labelled by $\mathcal{E}^{(0)}_{\pm}$. The interpretation of the amplitude $\mathcal{E}^{(0)}_{\pm}$ is that of a complex component of the Jones vector that varies when propagating along the fiber.

Field equations at $\mathcal{O}(\varepsilon)$ At first order in the slowness ε, the field equations reduce to inhomogeneous Bessel equations of the form

$$\underline{\mathbf{B}}_m a_b^{(1,m)} = 2i\beta\partial_\varsigma a_b^{(0,m)}\,, \tag{4.2.13}$$

where the inhomogeneity is given in terms of the zeroth order fields. The inhomogeneous solutions of an equation of the type

$$\mathcal{B}_m f = \psi(r)\,, \tag{4.2.14}$$

are

$$\mathbf{G}_m\left[\psi(r)\right] = \begin{cases} \mathbf{G}_m^{\text{core}}[\psi(r)] & r < 1\,, \\ \mathbf{G}_m^{\text{clad}}[\psi(r)] & r > 1\,, \end{cases} \tag{4.2.15}$$

where

$$\mathbf{G}_m^{\text{core}}[\psi(r)] = \frac{\pi}{2}\left(Y_m(Ur)\int_0^r J_m(Ur')\psi(r')r'\mathrm{d}r' + J_m(Ur)\int_r^1 Y_m(Ur')\psi(r')r'\mathrm{d}r'\right), \tag{4.2.16a}$$

$$\mathbf{G}_m^{\text{clad}}[\psi(r)] = -\left(I_m(Ur)\int_r^\infty K_m(Ur')\psi(r')r'\mathrm{d}r' + K_m(Ur)\int_1^r I_m(Ur')\psi(r')r'\mathrm{d}r'\right), \tag{4.2.16b}$$

for the core and the cladding respectively. The full solution takes the form

$$a^{(1,m)} = f_m(\mathbf{q}^{(1)}) - 2i\beta\underline{\mathbf{G}}[\partial_\varsigma a^{(0,m)}]\,, \tag{4.2.17}$$

where

$$\partial_\varsigma a^{(0,m)} = \partial_\varsigma f_m[\mathbf{q}^{(0)}]\,, \tag{4.2.18}$$

with the usual extension to frame components given by

$$\underline{\mathbf{G}}[a] = (\mathbf{G}_m a_0, \mathbf{G}_m a_s, \mathbf{G}_{m+1}a_\sharp, \mathbf{G}_{m-1}a_\flat)\,. \tag{4.2.19}$$

Jump conditions at $\mathcal{O}(\varepsilon)$ The interface conditions to first order in the slowness ε read

$$\mathbf{\Delta}[A]/e^{i(\psi(s)+m\theta-\omega t)} = \mathbf{M^0Nq^{(1)}} - 2i\beta\mathbf{\Delta}[\underline{\mathbf{G}}[\partial_\varsigma f_m[\mathbf{q}^{(0)}]]] + \mathcal{O}(\varepsilon^2) = 0\,, \tag{4.2.20}$$

where $\mathbf{M^0N}$ are the same as in the zeroth order case. The solution to the homogeneous part is derived in full analogy to the unperturbed case with the general solution given by

$$\mathbf{q}^{(1,\pm1)} = \mathcal{E}_\pm^{(1)}(\varsigma)\bar{\mathbf{q}}_\pm^{(1)}\,. \tag{4.2.21}$$

In that case, the inhomogeneous jumps from Eq. (4.2.20) must be contained in the image of $\mathbf{M^0N}$. This solvability requirement translates to the condition that

$$\hat{\mathbf{q}}\mathbf{\Delta}[\underline{\mathbf{G}}[\partial_\varsigma f_m[\mathbf{q}^{(0)}]]] = 0\,, \tag{4.2.22}$$

where

$$\hat{\mathbf{q}}^T = \begin{pmatrix} \zeta^{-2} \\ 0 \\ \frac{-i((\bar{n}V^2\mathcal{J}-\bar{m}W^2)n_1^2+(\bar{m}U^2+\bar{n}V^2\mathcal{K})n_2^2)}{\sqrt{2}(U^2\mathcal{J}+W^2\mathcal{K})(\bar{m}-\bar{n}(\mathcal{J}\mathcal{K})\omega n_1^2 n_2^2)} \\ \frac{i(-n_1^4 W^2\mathcal{J}+U^2\mathcal{K}n_2^4+n_1^2(\bar{m}\bar{n}V^2-(V^2\mathcal{J}+W^2(-\mathcal{J}+\mathcal{K}))n_2^2))}{\sqrt{2}(\bar{m}U^2-\bar{n}V^2\mathcal{K})(\bar{m}-\bar{n}(\mathcal{J}+\mathcal{K}))\omega n_1^2 n_2^2} \\ \frac{-i(W^2\mathcal{K}n_1^2+U^2\mathcal{J}n_2^2)(\bar{m}\bar{n}-\mathcal{J}n_1^2-\mathcal{K}n_2^2)V}{\sqrt{2}(U^2\mathcal{J}+W^2\mathcal{K})(\bar{m}-\bar{n}(\mathcal{J}+\mathcal{K}))\omega n_1^2 n_2^2\sqrt{W^2 n_1^2-U^2 n_2^2}} \\ 0 \\ \frac{i(U^2\mathcal{J}n_1^2+W^2\mathcal{K}n_2^2)}{(U^2\mathcal{J}+W^2\mathcal{K})\omega n_1^2 n_2^2} \\ -\frac{V^2}{(U^2\mathcal{J}+W^2\mathcal{K})\omega^2 n_1^2 n_2^2} \end{pmatrix}, \tag{4.2.23}$$

is a vector that spans the co-kernel of $\mathbf{M^0}$. Considering $m = \pm 1$ modes, Eq. (4.2.22) equates to

$$\partial_\varsigma \mathcal{E}_\pm^{(0)}(\varsigma) = 0\,, \tag{4.2.24}$$

implying that the complex amplitude $\mathcal{E}_\pm^{(0)}$ is independent of the long-distance scale ς.

Field equations at $\mathcal{O}(\varepsilon^2)$ The second order contribution of the field equations are of the form

$$\underline{\mathbf{B}}_m a_b^{(2,m)} = 2i\Sigma_b^m\,, \tag{4.2.25}$$

with respective inhomogeneities Σ_b^m (explicitly given in Appendix C), whose solutions take on the form

$$a^{(2,m)} = f_m(\mathbf{q}^{(2)}) - 2i\underline{\mathbf{G}}[\Sigma_b^m]\,. \tag{4.2.26}$$

Jump conditions at $\mathcal{O}(\varepsilon^2)$ At second order, the jumps of the solution are given by

$$\mathbf{\Delta}[A] = \mathbf{M^0}\mathbf{N}\mathbf{q^{(2)}} - 2i\mathbf{\Delta}[\underline{\mathbf{G}}[\Sigma_b^m]] + \mathbf{M^2}\mathbf{N}\mathbf{q^{(0)}} = 0\,, \tag{4.2.27}$$

where

$$\mathbf{M^2} = \begin{pmatrix} 0 & 0 & 0 & 0 & 0 & 0 & 0 & 0 \\ 0 & 0 & 0 & 0 & 0 & 0 & 0 & 0 \\ 0 & 0 & 0 & 0 & 0 & 0 & 0 & 0 \\ 0 & 0 & 0 & 0 & 0 & 0 & 0 & 0 \\ 0 & 0 & 0 & 0 & 0 & 0 & 0 & 0 \\ 0 & 0 & 0 & 0 & 0 & 0 & 0 & 0 \\ -in_1^2\zeta^{-3}\omega\nabla_+\nabla_-\zeta & 0 & 0 & 0 & in_2^2\zeta^{-3}\omega\nabla_+\nabla_-\zeta & 0 & 0 & 0 \\ 0 & 0 & 0 & 0 & 0 & 0 & 0 & 0 \end{pmatrix}, \tag{4.2.28a}$$

is an additional higher-order contribution that depends on the lapse function and second-order derivatives thereof. In analogy to the previous order, only mode values with $m = \pm 1$ provide a singular matrix $\mathbf{M^0N}$. Projecting onto the co-kernel

$$\hat{\mathbf{q}}^{(2)} \left(\mathbf{\Delta}[\underline{\mathbf{G}}[\Sigma_b^{\pm 1}]] + \frac{i}{2}\mathbf{M^2 N q^{(0)}} \right) = 0\,, \tag{4.2.29}$$

provides the solvability requirement, which implies an evolution equation for the first-order amplitudes. To see this, it is best to start by defining the complex vector

$$\mathcal{G} = \begin{pmatrix} \mathcal{E}_+ \\ \mathcal{E}_- \end{pmatrix}, \tag{4.2.30}$$

capturing the amplitudes of the $m = \pm 1$ modes. The implied evolution equation can then be written in the compact form

$$\frac{\mathrm{d}}{\mathrm{d}\varsigma}\mathcal{G}^{(1)}(\varsigma) = -i(\mathbf{B}(\varsigma) + \mathbf{C}(\varsigma))\mathcal{G}^{(0)}\,, \tag{4.2.31}$$

where the complex 2×2 matrices are given by

$$\mathbf{B}(\varsigma) = \begin{pmatrix} \alpha_1 R_{+-+-}(\varsigma) - 2\alpha_2 R_{+\|-\|}(\varsigma) & -\alpha_3 R_{+\|+\|}(\varsigma) \\ -\alpha_3 R_{-\|-\|}(\varsigma) & \alpha_1 R_{+-+-}(\varsigma) - 2\alpha_2 R_{+\|-\|}(\varsigma) \end{pmatrix}, \tag{4.2.32}$$

and

$$\mathbf{C}(\varsigma) = \begin{pmatrix} \alpha_4 \frac{\mathrm{d}^2}{\mathrm{d}\varsigma^2}\ln(\zeta(\varsigma)) + 2\alpha_5\nabla_+\nabla_-\zeta(\varsigma) & -\alpha_6\nabla_+\nabla_+\zeta(\varsigma) \\ -\alpha_6\nabla_-\nabla_-\zeta(\varsigma) & \alpha_4 \frac{\mathrm{d}^2}{\mathrm{d}\varsigma^2}\ln(\zeta(\varsigma)) + 2\alpha_5\nabla_+\nabla_-\zeta(\varsigma) \end{pmatrix}, \tag{4.2.33}$$

for some numerically obtained constants $\alpha_i \in \mathbf{R}$. Combining

$$\mathcal{G} = \mathcal{G}^{(0)} + \varepsilon\mathcal{G}^{(1)}\,, \tag{4.2.34}$$

and using $\varsigma = \varepsilon s$, Eq. (4.2.31) can be expressed as

$$\frac{\mathrm{d}}{\mathrm{d}s}\mathcal{J} = -i\varepsilon^2(\mathbf{B}+\mathbf{C})\mathcal{J}\,. \tag{4.2.35}$$

The slowness parameter may then be absorbed into the respective Riemann tensor components via $R_{abcd} = \varepsilon^2\tilde{R}_{abcd}$ and similarly for the second derivatives of the lapse function. Hence, by denoting $\varepsilon^2(\mathbf{B}+\mathbf{C}) = \mathbf{U}$, Eq. (4.2.35) can be expressed in the compact form

$$\frac{\mathrm{d}}{\mathrm{d}s}\mathcal{J}(s) = -i\mathbf{U}(s)\mathcal{J}(s)\,, \tag{4.2.36}$$

yielding an evolution equation for the Jones vector.

4.3 Summary

In the following, the main ideas of this chapter are conceptually summarized and outlined. Main assumptions:

- Metric expansion coefficients in (2.3.25) have characteristic length scales exceedingly higher than the optical wavelength.
- For the lapse function in Eq. (2.3.24a), only the $\mathcal{O}(\varepsilon^0)$ and $\mathcal{O}(\varepsilon^2)$ are taken into account.
- The shift vector in Eq. (2.3.24b) is set to $\xi = 0$.
- Higher-order fiber-bending corrections are neglected.
- Focus on SMF with a circular cross-section.

Using the multiple-scales expansion, the field equations reduce to (inhomogeneous) Bessel equations. At $\mathcal{O}(1)$ the field equations are homogeneous Bessel equations whose solvability is tied to the interface conditions. The mode solutions $m = \pm 1$ are given up to a scale-dependent amplitude $\mathcal{J}^{(0)}_{\pm}(\varsigma)$ which is determined by the next-order contribution.

In the leading order $\mathcal{O}(\varepsilon)$ the field equations are inhomogeneous Bessel equations, where the inhomogeneity is dependent on the previous order. The interface conditions for $m = \pm 1$ imply scale independence of the previous order amplitude, hence $\mathcal{E}^{(0)}_{\pm}(\varsigma) = \mathcal{E}^{(0)}_{\pm}$. The first-order amplitude $\mathcal{E}^{(1)}_{\pm}$ is determined by the next order.

The field equations at $\mathcal{O}(\varepsilon^2)$ are again given in terms of inhomogeneous Bessel equations, whose inhomogeneity depends on the $\mathcal{O}(1)$ and $\mathcal{O}(\varepsilon)$ contributions. The interface conditions in this case lead to an evolution equation for the first-order amplitude.

The two amplitudes for the $m = \pm 1$ modes can be regarded as the components of a complex two-vector, henceforward referred to as the Jones vector. More explicitly, the Jones vector is defined as $\mathcal{J} = (\mathcal{E}_+, \mathcal{E}_-)^{\mathrm{T}}$.

Assuming the Jones vector expands as $\mathcal{J} = \mathcal{J}^{(0)} + \varepsilon\mathcal{J}^{(1)} + \mathcal{O}(\varepsilon^2)$ leads to an evolution equation of the form

$$\frac{\mathrm{d}}{\mathrm{d}s}\mathcal{J}(s) = i\mathbf{U}(s)\mathcal{J}(s)\,, \tag{4.3.1}$$

whose interpretation will be discussed in the following chapter.

Chapter 5

Outline and results

At this stage, the evolution equation for the Jones vector is not yet fully interpretable. To this end, it is helpful to express the evolution equation in geometric terms, where the result can be expressed in terms of the Fermi-Walker transport discussed in Section 2.2.

5.1 Geometric (re-)formulation of Rytov's law

The evolution equation given in Eq. (4.3.1) is written in terms of a complex $\pm$-basis which was useful in the calculation process but is difficult to interpret geometrically. Thus, to obtain a geometric statement, all quantities appearing in Eq. (4.3.1) are reverted back to a Cartesian basis using Eq. (2.3.22). Furthermore by extending the two-dimensional Jones vector to three dimensions $\mathcal{J} = (\mathcal{J}_s, \mathcal{J}_x, \mathcal{J}_y)$, setting $\mathcal{J}_s = 0$, one arrives at

$$
\begin{aligned}
i\mathfrak{D}_s \mathcal{J}^k = \{(&\bar{\alpha}_1 R_{xyxy} + \bar{\alpha}_2 R_{msns}\delta^{mn} + \frac{\bar{\alpha}_5}{\zeta}\mathcal{P}^n{}_{k'}(\nabla^{k'}\nabla_n\zeta) + \bar{\alpha}_4 \nabla_s\nabla_s \ln\zeta)\delta^k{}_l \\
&+\bar{\alpha}_3(R^k{}_{sls} - \frac{1}{2}R_{msns}\delta^{mn}\delta^k{}_l) + \frac{\bar{\alpha}_6}{\zeta}(\mathcal{P}^k{}_{k'}(\nabla^{k'}\nabla_l\zeta) - \frac{1}{2}\delta^k{}_l\mathcal{P}^n{}_{k'}(\nabla^{k'}\nabla_n\zeta))\}\mathcal{J}^l \,,
\end{aligned}
\tag{5.1.1}
$$

with the projection operator given by

$$
\mathcal{P}^a{}_b = \delta^a{}_b - T^a T_b \,. \tag{5.1.2}
$$

Here, l_0 denotes the fiber's core radius, where the coupling moments are defined as $\hat{\alpha}_i = l_0\, \alpha_i$.

For Latin indices, the Einstein summation convention is used, summing over $\{x, y, s\}$, with the exception that x, y and s denote fixed components, respectively. Further, the baseline differential operator is readily expressed in terms of the Fermi-Walker derivative. Therefore, Eq. (5.1.1) provides an extension to Rytov's law in static curved space-times.

Interpretation The particular form of the equations allows for a distinction between phase-shift-induced contributions and complex polarization dynamics. To see this, define

$$\mathcal{H}_{\text{phase}} = \bar{\alpha}_1 \mathcal{K} + \bar{\alpha}_2 \text{Ric}_{ss} \delta^k{}_l + \frac{\bar{\alpha}_5}{\zeta} \mathcal{P}^n{}_{k'} (\nabla^{k'} \nabla_n \zeta) + \bar{\alpha}_4 \nabla_s \nabla_s \ln \zeta \,, \tag{5.1.3}$$

and

$$(\mathcal{H}_{\text{pol.}})^k_l = \bar{\alpha}_3 (R^k{}_{sls} - \frac{1}{2} \text{Ric}_{ss} \delta^k{}_l) + \frac{\bar{\alpha}_6}{\zeta} (\mathcal{P}^k{}_{k'} \nabla_l \zeta) - \frac{1}{2} \delta^k{}_l \mathcal{P}^n{}_{k'} (\nabla^{k'} \nabla_n \zeta)) \,, \tag{5.1.4}$$

where $\mathcal{K} = R_{xyxy}$ denotes the sectional curvature and $\text{Ric}_{ss} = R_{msns} \delta^{mn}$ denotes the ss-component of the Ricci curvature tensor. This allows for Eq. (5.1.1) to be expressed in the concise form

$$i \mathfrak{D}_s \mathcal{G}^k = \mathcal{H}_{\text{phase}} \, \mathcal{G}^k + \mathcal{H}_{\text{pol.}}{}^k{}_l \, \mathcal{G}^l \,, \tag{5.1.5}$$

which provides an extension to Rytov's law for optical fibers in the absence of fiber bending. Here, $\mathcal{H}_{\text{phase}}$ induces pure phase shifts and hence admits phase-like solutions. On the other hand, the matrix $\mathcal{H}_{\text{pol.}}$ induces complex polarization dynamics including contributions that are linked to phase shifts. This can be inferred from the fact that its components are trace-free.

All quantities appearing in both matrices are very small and unfeasible with current experimental sensitivity. To provide the most likely prediction, for which experimental measurements are sensitive enough, it is necessary to look at the order of magnitude of the coupling constants.

5.2 Frequency dependence in single-mode fibers

In the following, the numerical values for the coupling constants in the normalized frequency range $V \in (0, 10)$ are analyzed.

The frequency dependence of the coupling constants, related to phase contributions of the matrix $\mathcal{H}_{\text{phase}}$, is provided in Figs. 5.1 to 5.3.

Numerical plots of the coupling constants of $\mathcal{H}_{\text{pol.}}$ contributing to polarization dynamics are provided in Fig. 5.4. The gray shaded areas in Figs. 5.1 to 5.4 mark the single-mode regime in accordance to Fig. 3.1, whereas the dashed blue line indicates the operating normalized frequency of a specific type of single-mode fiber (SMF-28e), typically used in experimental setups. The fiber specifications and the corresponding values for the coupling constants are summarized in Table 5.1. Furthermore, to illustrate the difference in magnitude of the coupling constants a logarithmic plot is provided in Fig. 5.5.

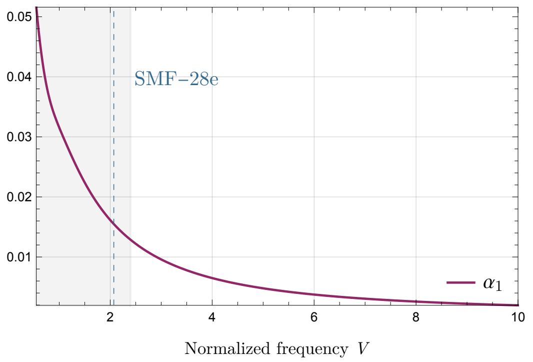

Figure 5.1: Phase coupling constant α_1.

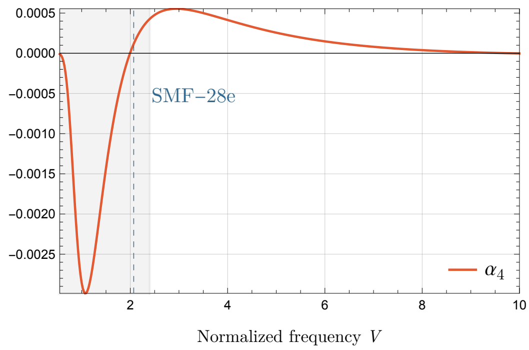

Figure 5.2: Phase coupling constant α_4.

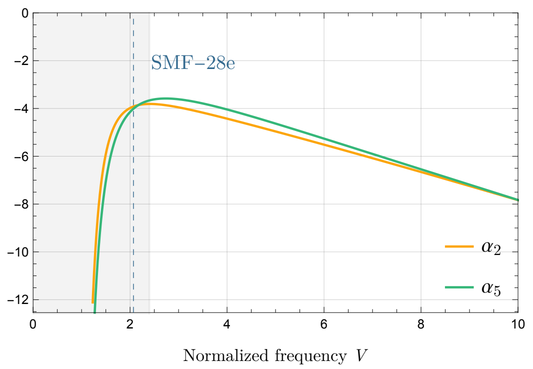

Figure 5.3: Phase coupling constants α_2 and α_5.

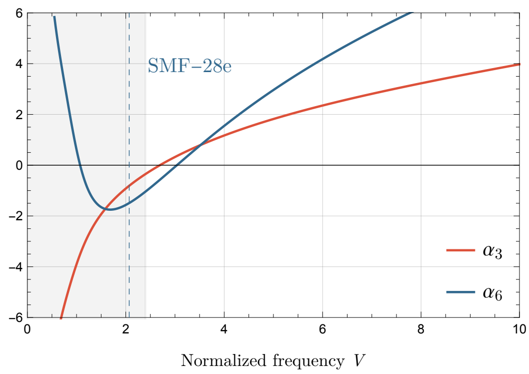

Figure 5.4: Polarization coupling constants α_3 and α_6.

Interpretation Quantities such as components of the Riemann curvature tensor and second derivatives of the lapse function, are of pure geometrical origin and therefore expected to be very small in magnitude but roughly of the same order. This means that the coupling constants are a good indicator to isolate the most dominant quantities. Considering SMF-28e fibers, Table 5.1 shows that phase terms such as the coupling to the *ss*-component of the Ricci tensor or second transverse derivatives of the lapse function appear to have the highest values of coupling constants (see also Fig. 5.5) and are therefore more likely to be detectable in future experiments.

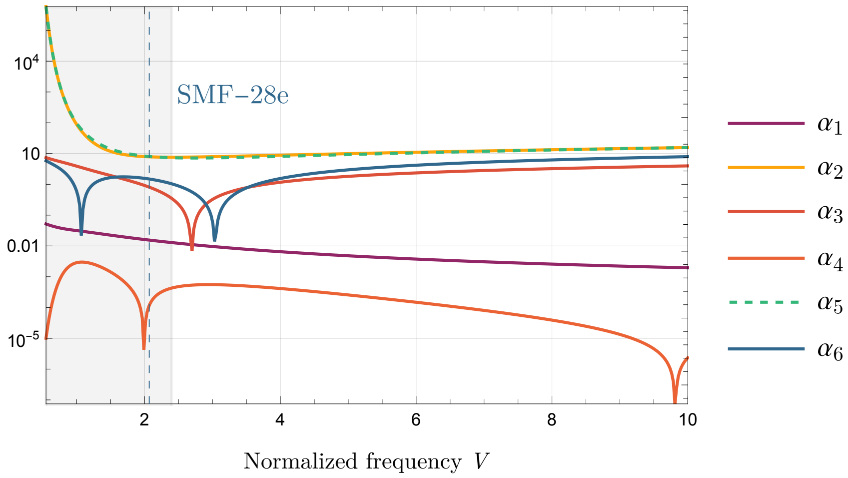

Figure 5.5: Logarithmic plot of absolute values of the coupling constants. The grey shaded area marks the single-mode regime while the dashed blue line marks a commercially available single-mode fiber (SMF-28e).

Parameter	Symbol	Value	Parameter	Symbol	Value
Core Radius	ϱ	4μm	Sectional phase	$\alpha_{\text{1-ph-Sec}}$	0.016
Wavelength	λ	1550nm	Ricci phase	$\alpha_{\text{2-ph-Ricc}}$	-3.981
Core Refractive Index	n_1	1.4712	Riem. pol.	$\alpha_{\text{3-pol-R}}$	-0.921
Cladding Refractive Index	n_2	1.4659	Lapse long. ph.	$\alpha_{\text{4-ph-}\zeta}$	10^{-5}
Normalized Frequency	V	2.069	Lapse tr. ph.	$\alpha_{\text{5-ph-dd}\zeta}$	-4.146
Normalized Guide Index	$b(V)$	0.4371	Lapse tr. pol.	$\alpha_{\text{6-pol-dd}\zeta}$	-1.567

Table 5.1: Numerical single-mode fiber parameters for $m = 1$.

5.2.1 Example

In general, all results so far hold without imposing Einstein's field equations. In the case where Einstein's equations are imposed, Eq. (5.1.5) can be simplified using the relations

$$\Delta\zeta = 0\,, \qquad \nabla_i\nabla_j\zeta = \zeta^{-1}\mathrm{Ric}_{ij}\,, \tag{5.2.1}$$

where Latin indices denote spatial coordinates [58]. Then Eq. (5.1.5) reads

$$\begin{aligned} i\mathfrak{D}_s\mathcal{J}^k &= \left[\frac{\alpha_1}{4}\mathcal{K} + \alpha_{\text{comb.}}\mathrm{Ric}(T,T)\right]\mathcal{J}^k \\ &\quad + \left[\alpha_4 R^k{}_{ilj}T^iT^j + \alpha_6\mathrm{Ric}^k{}_l\right]\mathcal{J}^l\,, \end{aligned} \tag{5.2.2}$$

where $\alpha_{\text{comb.}} = \alpha_2 - \alpha_5 + \frac{1}{2}(\alpha_6 + \alpha_3)$. To study a fiber under the influence of Earth's gravitational field, the metric may be expressed in terms of the linearized post-Newtonian metric given by

$$g_{\mathtt{PN}} = -(1 - 2\psi)\mathrm{d}t^2 + (1 + 2\psi)(\mathrm{d}x^2 + \mathrm{d}y^2 + \mathrm{d}z^2)\,, \tag{5.2.3}$$

with ψ denoting the gravitational potential [59]. In the present case, the shift vector is neglected and the gravitational potential ψ is given by

$$\psi = \psi(x, y, z) = -\frac{\mathrm{GM}}{r}\,, \tag{5.2.4}$$

where $r = \sqrt{x^2 + y^2 + z^2}$, G denoting the gravitational constant and M representing Earth's mass. In the following, the values of the coupling constants are set to values appearing in the right column of Table 5.1.

Closed loop around Earth Consider the curve

$$\gamma(\varsigma) = r\left(\cos\left(\frac{\varsigma}{r}\right)\sin\left(\theta(L)\right), \sin\left(\frac{\varsigma}{r}\right)\sin\left(\theta(L)\right), \cos\left(\theta(L)\right)\right)\,, \tag{5.2.5}$$

with the constant azimuthal angle given by

$$\theta(L) = \arcsin\left(\frac{L}{R_\oplus 2\pi\left(1 - \frac{1}{2}\psi\right)}\right)\,, \tag{5.2.6}$$

for fixed fiber length L, where $R_\oplus$ denotes Earth's radius. Note that the parameter ς is, for the metric given in Eq. (5.2.3), related to the physical arc-length s by

$$\frac{\mathrm{d}\varsigma}{\mathrm{d}s} = \left(\sqrt{g_{\mathtt{PN}}(\dot{\gamma}, \dot{\gamma})}\right)^{-1}\,. \tag{5.2.7}$$

To solve Eq. (5.2.2) for the Jones vector, it is necessary to specify the initial conditions. In all generality, an initial Jones vector $\mathcal{J}(0)$, in a chosen basis, following the light propagation of a fiber with length L, will evolve according to

$$\mathcal{J}(\varsigma) = \mathbf{E}(\varsigma)\mathcal{J}(0)\,, \tag{5.2.8}$$

where $\mathbf{E}(\varsigma)$ represents an evolution matrix for the polarization states. Inserting into Eq. (5.2.2) implies an evolution for the evolution matrix of the form

$$\mathfrak{D}_s\mathbf{E}(\varsigma) = -i\mathcal{H}\mathbf{E}(\varsigma)\,, \tag{5.2.9}$$

where $\mathcal{H}$ captures the right-hand side of Eq. (5.2.2). Note that for Rytov's law, $\mathbf{E}(\varsigma)$ reduces to the identity matrix. Solving Eq. (5.2.9) for a fiber laid out in a closed loop with fiber-length $L = 1\,\mathrm{m}$ yields

$$\mathbf{E}(2\pi) = \begin{pmatrix} 1 - 5i \cdot 10^{-16} & 0 & 2i \cdot 10^{-23} \\ 0 & 0 & 0 \\ 2i \cdot 10^{-23} & 0 & 1 + 3i \cdot 10^{-16} \end{pmatrix} . \tag{5.2.10}$$

Hence, Eq. (5.2.10) determines the evolution of any initial polarization configuration of the Jones vector according to Eq. (5.2.8).

Circularly polarized initial conditions The initial Jones vector describing right circularly polarized light traveling in y-direction is given by

$$\mathcal{J}(0) = (1, 0, -i)^T . \tag{5.2.11}$$

Using Eq. (5.2.10), the initial state, after a full rotation of 2π, reads

$$\mathcal{J}(2\pi) = (1 - 5 \cdot 10^{-16} i,\, 0,\, 3 \cdot 10^{-16} - i)^T . \tag{5.2.12}$$

Any additional loop can be calculated by taking powers of the evolution matrix. For example, consider $4 \cdot 10^4$ revolutions, then

$$\mathbf{E}(4 \cdot 10^4 \cdot 2\pi) = (\mathbf{E}(2\pi))^{4 \cdot 10^4} = \begin{pmatrix} 1 - 2i \cdot 10^{-11} & 0 & 8i \cdot 10^{-19} \\ 0 & 0 & 0 \\ 8i \cdot 10^{-19} & 0 & 1 + i \cdot 10^{-11} \end{pmatrix} . \tag{5.2.13}$$

The evolved Jones vector is then given by

$$\mathcal{J}(4 \cdot 10^4 \cdot 2\pi) = (1 - 2 \cdot 10^{-11} i,\, 0,\, 1 \cdot 10^{-11} - i)^T . \tag{5.2.14}$$

Interpretation Starting from circularly polarized light, the Jones vector is evolved using the transport equation given in Eq. (5.2.2) for a fiber with physical length $1\,\mathrm{m}$. As a result, the Jones vector experiences a small correction in its transverse components, while maintaining orthogonality to the direction of propagation (y-direction). The correction to the x-component of the Jones vector features a small phase shift, whereas the correction to the z-component can be interpreted as a small perturbation. This perturbation induces a slight change from circular polarization to elliptical polarization.

In comparison to the case, where the fiber is laid out in a loop, any additional revolution increases the order of magnitude of the phase shift by the order of magnitude of the number of turns considered. The elliptical perturbation, on the other hand, features an increase that is one order of magnitude smaller compared to the phase contributions (compare Eqs. (5.2.10) and (5.2.13)).

Note that in the absence of space-time curvature, the evolution equation reduces to

Rytov's law, where the Jones vector remains constant along the entire curve.

Chapter 6

Discussion

In this work, a modification of Rytov's law for single-mode step-index fibers in a curved space-time has been derived from the full Maxwell equations, where a perturbative multiple-scales method was used. The corrections that arise from space-time curvature are characterized by 6 coupling constants associated with second derivatives of the lapse function as well as spatial Riemann and spatial Ricci tensor curvature contributions. The frequency dependent coupling moments $\bar{\alpha}_1$, $\bar{\alpha}_2$, $\bar{\alpha}_4$ and $\bar{\alpha}_5$ are associated with phase shifts whereas $\bar{\alpha}_3$ and $\bar{\alpha}_6$ introduce complex polarization dynamics. The methods used to derive the evolution equation allow for a variation in refractive index as well as fiber core radius and frequency. Hence, the evolution equation is expected to be capable of describing a variety of different single-mode fibers.

The equations derived in the thesis at hand provide an extension to the equations derived by Mieling, in the case of a static space-time [17]. In this setting, his thesis qualitatively described the structure of the appearing equations following a similar perturbative scheme. In his thesis, Mieling further provided a full characterization of terms that are expected to appear at different orders in the expansion with corresponding Fourier mode coupling, which, on the one hand, served as a main motivation for this thesis and on the other hand, the present work confirms their appearance.

In a previous paper, Mieling and Oancea already extended Rytov's law, where higher order fiber bending corrections are derived in flat space-time for single-mode step-index fibers [20]. These bending corrections are specified by a phase curvature moment η as well as a polarization curvature moment ξ. By setting the lapse function $\zeta = 1$, the present work can be viewed as an extension of the bending corrections. Since the work by Mieling and Oancea considered single-mode step-index fibers and their derivation is based on an analogous weak bending assumption, combining both works leads to a full characterization of the response of the electromagnetic field to weakly bent fibers in an arbitrarily curved space.

Quantum communication remains a highly active field of research where the degrees of freedom of a photon, such as the polarization, allow for a transmission of information.

In the space-time context, a natural question to ask would be how space-time curvature affects a wave packet traveling through space-time. The 2021 article by Exirifard *et al.* aims to answer this question, where they analyzed relativistic wave packets traveling along arbitrary null geodesics. They showed that, indeed, the space-time curvature contributions coming from the Riemann curvature tensor result in a distortion of the wave packet [60]. However, in the work at hand, wave packets are considered to be guided along the fiber core and hence traveling along time-like curves. It is worth noting that, although the space-time may be arbitrary, fiber optics is tied to local applications. Therefore, any transmission of light using fibers on cosmological or solar length scales is unlikely due to information loss [61].

6.1 Outlook

Fiber model Even though the corrections to Rytov's law in this thesis are derived to describe polarization dynamics of light in a realistic step-index fiber model there is still room for improvement on the model assumptions. For example, the fiber is modeled as a cylindrical waveguide with a perfectly circular cross-section. Although this may seem sufficient for all practical purposes, in reality, elastic deformation of the fiber's cross-section causes linear birefringence and therefore impacts the polarization dynamics [62]. There might be the possibility to consider liquid core fibers, for which the cross-section deformations can be neglected [63]. However, the methods presented in this work would need to be supplemented by equations governing the flow of liquids. Furthermore, an experimental fiber setup may be subject to temperature fluctuations, which impact the fiber's material properties and ultimately affect the core and cladding material causing a change in refractive index [64; 65].

Space-time assumptions In the setting of a static space-time, future contributions should include first-order derivatives of the lapse function, which are neglected in the present work. These additional terms require more elaborate calculations, similar to quadratic bending corrections derived in [20]. Therefore, future models have to account for the bending corrections as well as the first-order lapse contributions in a combined framework. The lapse function enters via the metric and therefore impacts the field equations and the interface conditions, meaning that the curvature moments and the bending corrections, derived by Mieling and Oancea in the flat space-time setting, might deviate from the general space-time case.

A further attempt to advance the model is to consider a stationary space-time. In this setting, one introduces the time-independent shift vector field. This has already been considered by Mieling. He derived an extension to Rytov's law starting from the ADM metric, where the shift vector was considered to appear only linearly. In this setting, not only the gravitational redshift, captured by the lapse function, can be investigated, but also the Sagnac effect, which is related to the shift vector [17].

Lastly, the space-time may altogether be considered dynamical, allowing for a time-dependent lapse function and a time-dependent shift vector field (discussed in Appendix A). In the case where the lapse function is time-dependent, one needs to construct a different transport equation (see Appendix A.3). However, in this case, the metric (see Eq. (A.3.11)) features quantities for which one needs additional input such as the four-velocity, its parallel transport and its rate of change in the tangential direction, similarly for the transverse directions.

In practice one faces the problem of formulating a plausible dynamical model describing an optical fiber. Such a model has to account for dynamic changes in the refractive index and variations of the core-cladding interface. A full dynamical formulation of an optical fiber is therefore an open problem and needs further investigation.

Appendix A

Static vs. dynamical space-time

In Section 2.3 the metric expansion is derived on a static space-time, e.g., where the Killing vector field is hypersurface-orthogonal. This section aims to display the difficulties that arise when the space-time under consideration is dynamic. To this end, the metric will be derived up to the first order in the separation of a two-surface. Ultimately a transport equation for the frames is derived, where additional input is required for further computations.

A.1 Dynamical space-time setup

The main construction starts by considering a semi-Riemannian manifold $\mathscr{M}$ and a time-like two-surface $\mathscr{W}$ embedded in $\mathscr{M}$ by $\mathscr{W} \overset{\imath}{\hookrightarrow} \mathscr{M}$. This two-surface can be thought of as the world-sheet traced out by the baseline of an optical fiber. Being a material object, the fiber has a four-velocity u with corresponding one-form $\flat_g(u)$, where $\flat_g$ denotes the musical isomorphism map with respect to the space-time metric g. In general,

$$\flat_g(u) \wedge \mathrm{d}(\flat_g(u)) \neq 0\,, \tag{A.1.1}$$

meaning u need not be hypersurface-orthogonal. However, by defining $\vartheta := \imath^*(\flat_g(u))$ on $\mathscr{W}$, then by definition

$$\vartheta \wedge \mathrm{d}\vartheta = 0\,, \tag{A.1.2}$$

holds. Eq. (A.1.2) is satisfied on $\mathscr{W}$, since the wedge product of the one-form ϑ with its exterior derivative $\mathrm{d}\vartheta$ yields a three-form which is zero on a two-surface. Furthermore, the Frobenius theorem states that if and only if Eq. (A.1.2) holds, then locally there are functions ζ and t such that

$$\vartheta = -\zeta \mathrm{d}t\,, \tag{A.1.3}$$

holds [66]. For $\zeta \neq 0$ everywhere t defines a foliation on $\mathscr{W}$ into hypersurfaces Σ_t for each value of t. Therefore, the integrability condition Eq. (A.1.2) gives rise to adapted coordinates (t, s) on $\mathscr{W}$ for which $\bar{g}(dt, ds) = 0$. The corresponding four-velocity vector field is given by

$$v = \sharp(\vartheta) = \frac{1}{\zeta(t,s)} \partial_t \,, \tag{A.1.4}$$

with normalization $g(v, v) = -1$ and such that $g(\partial_t, \partial_s) = 0$. Note that, while here the components of v are defined w.r.t. $\mathscr{W}$, there is no difference between v and u on $\mathscr{M}$, thus, in the following, one writes u when the four-velocity is considered. The metric on $\mathscr{W}$ is given by

$$g_{\mathscr{W}} = -\zeta^2(t,s) dt^2 + g_{ss}(t,s) ds^2 \,. \tag{A.1.5}$$

A.2 Metric expansion on a dynamical space-time

To begin with, let $\mathscr{M}$ be a four-dimensional Lorentzian manifold with metric g. The construction of Fermi normal coordinates is analogous to Section 2.2. The orthonormal frame $(\mathfrak{e}_t.\mathfrak{e}_s, \mathfrak{e}_i)$ together with function

$$\psi = \exp_p(x^i \mathfrak{e}_i(t,s)) \,, \tag{A.2.1}$$

where p is the point that corresponds to the coordinates (t, s) on $\mathscr{W}$, gives rise to a coordinate system $\mathscr{S} = (t, x^i, s)$. In these coordinates, the vector fields ∂_α are orthogonal along $\mathscr{W}$. The metric expansion around the two-surface in the transverse directions is of the form

$$g = g|_{\mathscr{W}} + (\partial_k g)|_{\mathscr{W}} x^k + \mathscr{O}(r^2) \,, \tag{A.2.2}$$

where again $r^2 = (x^1)^2 + (x^2)^2$. The zeroth order metric expansion of Eq. (A.2.2) is given by

$$g|_{\mathscr{W}} = g_{\mathscr{W}} + (\mathrm{d}x^1)^2 + (\mathrm{d}x^2)^2 \,, \tag{A.2.3}$$

where $g_{\mathscr{W}}$ is the metric of $\mathscr{W}$ as in Eq. (A.1.5). By expressing each component of the metric separately in terms of Christoffel symbols, the first-order correction yields

$$\partial_k g_{tt} = 2\Gamma_{ttk} \,, \qquad \partial_k g_{ts} = 2\Gamma_{tsk} \,, \qquad \partial_k g_{st} = 2\Gamma_{stk} \,, \qquad \partial_k g_{ti} = 2\Gamma_{tik} \,, \tag{A.2.4a}$$

$$\partial_k g_{it} = 2\Gamma_{itk} \,, \qquad \partial_k g_{ss} = 2\Gamma_{ssk} \,, \qquad \partial_k g_{si} = 2\Gamma_{sik} \,, \qquad \partial_k g_{is} = 2\Gamma_{isk} \,, \tag{A.2.4b}$$

$$\partial_k g_{ij} = \Gamma_{ijk} \,, \qquad \partial_k g_{ji} = \Gamma_{jik} \,, \tag{A.2.4c}$$

here the evaluation on the two-surface is suppressed for brevity. This can be reduced by using Eq. (2.3.9). Define a family of geodesics by

$$\gamma^\mu(\lambda, t, s) = \lambda \left(\kappa_\perp^\mu + (t+s)\eta_\perp^\mu\right) + s\eta_\parallel^\mu + t\eta_t^\mu\,, \tag{A.2.5}$$

where (t, s) parametrize the curves and λ being the affine parameter, with velocity vector field given by

$$\kappa_\perp^\mu = \text{constant}\,. \tag{A.2.6}$$

Using the auto-parallel equation gives

$$\Gamma_{\alpha ij}|_{\mathscr{W}} = 0\,. \tag{A.2.7}$$

The only potentially non-trivial metric derivatives are given by

$$\partial_k g_{tt} = 2\Gamma_{ttk}\,, \qquad \partial_k g_{ts} = 2\Gamma_{tsk}\,, \qquad \partial_k g_{st} = 2\Gamma_{stk}\,, \tag{A.2.8a}$$
$$\partial_k g_{it} = 2\Gamma_{itk}\,, \qquad \partial_k g_{ss} = 2\Gamma_{ssk}\,, \qquad \partial_k g_{is} = 2\Gamma_{isk}\,, \tag{A.2.8b}$$

where the evaluation $\mathscr{W}$ is suppressed for readability. Along the tangential directions

$$\nabla_{\partial_t} g(\partial_s, \partial_k) = \nabla_{\partial_s} g(\partial_t, \partial_k) = 0\,, \tag{A.2.9}$$

is satisfied, and it follows $\Gamma_{stk} = \Gamma_{tsk}$. Further, using

$$\nabla_{\partial_t} g(\partial_k, \partial_i) = \nabla_{\partial_s} g(\partial_k, \partial_i) = 0\,, \tag{A.2.10}$$

implies $\Gamma_{itk} = -\nabla_{\partial_k} g(\partial_i, \partial_t)$ and $\Gamma_{isk} = -\nabla_{\partial_k} g(\partial_i, \partial_s)$. Expressing the metric as

$$\partial_k g_{tt} = 2g(\partial_t, \nabla_{\partial_t}\partial_k)\,, \quad \partial_k g_{st} = 4g(\partial_s, \nabla_{\partial_t}\partial_k)\,, \quad \partial_k g_{ss} = 2g(\partial_s, \nabla_{\partial_s}\partial_k)\,, \tag{A.2.11a}$$
$$\partial_k g_{it} = 2g(\partial_i, \nabla_{\partial_t}\partial_k)\,, \quad \partial_k g_{is} = 2g(\partial_i, \nabla_{\partial_s}\partial_k)\,, \tag{A.2.11b}$$

yields the following general expression of the metric expansion as

$$\begin{aligned} g(t, s, x^i) \simeq &- \left(g_{tt}(t, s) + 2\Gamma_{ttk}|_{\mathscr{W}} x^k\right) \mathrm{d}t^2 + \left(g_{ss}(t, s) + 2\Gamma_{ssk}|_{\mathscr{W}} x^k\right) \mathrm{d}s^2 \\ &+ \left(4\Gamma_{tsk}|_{\mathscr{W}} x^k\right) \mathrm{d}t\mathrm{d}s + \left(2\Gamma_{itk}|_{\mathscr{W}} x^k\right) \mathrm{d}x^i\mathrm{d}t + \left(2\Gamma_{isk}|_{\mathscr{W}} x^k\right) \mathrm{d}x^i\mathrm{d}s \\ &+ \mathrm{d}x^2 + \mathrm{d}y^2\,. \end{aligned} \tag{A.2.12}$$

A.3 Constructing a transport equation

In Eq. (A.2.12) the quantities $\nabla_{\partial_t}\partial_k$, $\nabla_{\partial_s}\partial_k$ and $\nabla_{\partial_s}\partial_t$ remain unspecified and need additional input. Therefore, to reduce the problem at hand in complexity, in analogy to Section 2.2, it is necessary to construct a transport equation for $\nabla_{\partial_s}\partial_k$. All the abovelisted quantities are evaluated on $\mathscr{W}$. Hence, $\partial_\alpha = \mathfrak{e}_\alpha$, with $\mathfrak{e}_\alpha$ being defined only on $\mathscr{W}$, whereas ∂_α also being defined in an open neighborhood around $\mathscr{W}$. In the following the expressions of $\mathfrak{e}_\alpha$ and ∂_α are used interchangeably where appropriate. In general, ∂_s is not normalized, hence

$$g(\partial_s, \partial_s) = \tau^2(t,s)\,, \tag{A.3.1}$$

where $\tau(t,s)$ is some function on $\mathscr{W}$. The unit vector along ∂_s is given by

$$T = \frac{1}{\tau(t,s)}\partial_s\,, \tag{A.3.2}$$

such that $g(T,T) = 1$. This implies

$$\nabla_T \partial_k = \frac{1}{\tau(t,s)}\nabla_{\partial_s}\partial_k = \frac{1}{\tau(t,s)}\Gamma^\alpha_{sk}\partial_\alpha\,. \tag{A.3.3}$$

The normal is then given by $\nu = \nabla_T T$. The most general transport that can be constructed is of the form

$$\nabla_{\partial_s}\partial_k = C^k\partial_k + A\partial_s + B\partial_t\,, \tag{A.3.4}$$

for some coefficients A, B and C. The coefficients are determined by requiring orthogonality of the vector fields and hence are given by

$$A = \Gamma^s_{sk} = -\frac{\Gamma_{kss}}{g(\partial_s,\partial_s)} = -\frac{1}{\tau^2}\Gamma_{kss} = -\frac{1}{\tau^2}g(\nabla_{\partial_s}\partial_s, \partial_k) = -g(\nabla_T T, \partial_k) \tag{A.3.5a}$$

$$B = \Gamma^t_{sk} = -\frac{\Gamma_{kst}}{g(\partial_t,\partial_t)} = \frac{1}{\zeta^2}\Gamma_{kst} = \frac{1}{\zeta^2}g(\nabla_{\partial_s}\partial_t, \partial_k) = g(\nabla_{\partial_s}u, \partial_k) \tag{A.3.5b}$$

$$C_k = \tau(t,s)\Gamma_{ksi}\,. \tag{A.3.5c}$$

With this at hand, a transport equation can be defined by its action on a vector field h by

$$\mathscr{D}h := \nabla_T h + g(\nu,h)T - g(T,h)\nu - \zeta(t,s)\left[g(\nabla_T u, h)u - g(u,h)\nabla_T u\right]\,. \tag{A.3.6}$$

It is readily verified that $\mathscr{D}g = 0$ is satisfied. Acting with Eq. (A.3.6) on the frame gives

$$\mathscr{D}\mathfrak{e}_k = \tau(t,s)\Gamma^i_{sk}\partial_i\,. \tag{A.3.7}$$

The action of Eq. (A.3.7) on the tangential directions yields

$$\mathscr{D}T = -\zeta g(\nabla_T u, T)u\,, \tag{A.3.8a}$$

as well as

$$\mathscr{D}u = \nabla_T u + g(\nu, u)T - \zeta(t,s)\left[g(\nabla_T u, u)u - g(u,u)\nabla_T u\right] . \tag{A.3.8b}$$

Now, under the assumption that $\mathfrak{e}_k$ is chosen such that $\mathscr{D}\mathfrak{e}_k = 0 \Leftrightarrow \Gamma_{isk} = 0$, applying Eq. (A.3.7) leads to

$$\nabla_T \mathfrak{e}_k = -g(\nu, \mathfrak{e}_k)T + \zeta g(\nabla_T u, \mathfrak{e}_k)u = -\frac{1}{\tau}\Gamma_{kss}T + \frac{1}{\tau}\Gamma_{kst}u \, . \tag{A.3.9}$$

Furthermore, defining $\nu = \nu^\alpha \partial_\alpha$ and $\nabla_T u = (\nabla_T u)^\alpha \partial_\alpha$ implies

$$\Gamma_{ssk} = -\tau^2(t,s)\nu_k \, , \tag{A.3.10a}$$

as well as

$$\Gamma_{tsk} = -\tau(t,s)\zeta(t,s)(\nabla_T u)_k \, . \tag{A.3.10b}$$

Lastly, setting $\Gamma_{ttk} = -\zeta^2(\nabla_u u)_k$ and $\Gamma_{itk} = -\zeta(\nabla_u \mathfrak{e}_i)_k$, leads to the following form of the metric

$$\begin{aligned} g(t,s) \simeq & -\zeta(t,s)^2\left(1 - 2(\nabla_u u)_k x^k\right)\mathrm{d}t^2 + \tau(t,s)^2\left(1 - 2\nu_k x^k\right)\mathrm{d}s^2 \\ & - 4\tau(t,s)\zeta(t,s)\left((\nabla_T u)_k x^k\right)\mathrm{d}t\mathrm{d}s - 2\zeta(t,s)\left((\nabla_u \mathfrak{e}_i)_k x^k\right)\mathrm{d}x^i\mathrm{d}t \\ & + \mathrm{d}x^2 + \mathrm{d}y^2 \, . \end{aligned} \tag{A.3.11}$$

Appendix B

Multiple-scales method for coupled oscillators

This chapter serves as a toy model for the actual problem considered in this thesis, as well as an illustration of the multiple-scales method.

Consider the following system of coupled oscillators

$$\ddot{x}(t) + x(t) - \epsilon^2 h(\epsilon t) y(t) = 0\,, \ \ \ddot{y}(t) + y(t) - \epsilon^2 h(\epsilon t) x(t) = 0\,, \tag{B.0.1a}$$

for some coupling function $h(\epsilon t)$ and small coupling parameter ϵ. The slowly varying function

$$\tau(t) = \int_0^t \nu(\epsilon t')\mathrm{d}t'\,, \tag{B.0.2}$$

gives rise to a slow timescale denoted by

$$\sigma = \epsilon^2 \tau(t)\,. \tag{B.0.3}$$

The multiple-scales ansatz of the solution reads

$$f_i(t) = f_i^{(0)}(t,\sigma) + \epsilon^2 f_i^{(1)}(t,\sigma) + \mathcal{O}(\epsilon^3)\,, \tag{B.0.4}$$

where $f_i = (x, y)$. Inserting Eq. (B.0.4) into Eq. (B.0.1) one finds

$$\epsilon^0 : \quad \ddot{x}^{(0)}(t,\sigma) + x^{(0)}(t,\sigma) = 0\,, \tag{B.0.5}$$

$$\ddot{y}^{(0)}(t,\sigma) + y^{(0)}(t,\sigma) = 0\,, \tag{B.0.6}$$

$$\epsilon^2 : \quad \ddot{x}^{(1)}(t,\sigma) + x^{(1)}(t,\sigma) = -h(\epsilon t) y^{(0)}(t,\sigma) + 2\nu(\epsilon t)\partial_\sigma \dot{x}^{(0)}, \tag{B.0.7}$$

$$\ddot{y}^{(1)}(t,\sigma) + y^{(1)}(t,\sigma) = -h(\epsilon t) x^{(0)}(t,\sigma) + 2\nu(\epsilon t)\partial_\sigma \dot{y}^{(0)}\,, \tag{B.0.8}$$

where $\dot{a}$ denotes the derivative w.r.t. the variable t. The zeroth order solutions

$$f_i^{(0)} = A_i(\sigma)e^{it} + B_i(\sigma)e^{-it}\,, \tag{B.0.9}$$

are that of a simple harmonic oscillator where the coefficients still depend on the slow timescale σ. Due to the coupling of Eq. (B.0.1) being of order ϵ^2, there are no first-order terms. However, at second-order in the expansion, inhomogeneities appear. Solvability of the $\mathcal{O}(\varepsilon^2)$ means

$$-h(\epsilon t)y^{(0)}(t,\sigma) + 2\nu(\epsilon t)\partial_\sigma \dot{x}^{(0)} = 0\,, \tag{B.0.10a}$$

as well as

$$-h(\epsilon t)x^{(0)}(t,\sigma) + 2\nu(\epsilon t)\partial_\sigma \dot{y}^{(0)} = 0\,, \tag{B.0.10b}$$

and is therefore tied to a choice for $\nu(\epsilon t)$. Setting $\nu(\epsilon t) = -\frac{1}{2}h(\epsilon t)$ and inserting Eq. (B.0.9) into Eq. (B.0.10) leads to

$$e^{it}\left(\partial_\sigma A_1(\sigma) - iA_2(\sigma)\right) - e^{-it}\left(\partial_\sigma B_1(\sigma) - iB_2(\sigma)\right) = 0\,, \tag{B.0.11a}$$

$$e^{it}\left(\partial_\sigma A_2(\sigma) - iA_1(\sigma)\right) - e^{-it}\left(\partial_\sigma B_2(\sigma) - iB_1(\sigma)\right) = 0\,, \tag{B.0.11b}$$

with general solutions

$$A_1(\sigma) = c_1\cos(\sigma) + ic_2\sin(\sigma)\,, \quad B_1(\sigma) = c_3\cos(\sigma) - ic_4\sin(\sigma)\,, \tag{B.0.12a}$$

$$A_2(\sigma) = c_2\cos(\sigma) + ic_1\sin(\sigma)\,, \quad B_2(\sigma) = c_4\cos(\sigma) - ic_3\sin(\sigma)\,. \tag{B.0.12b}$$

To express the general solution of Eq. (B.0.1) in a compact form, define

$$\mathbf{R}_\pm(\sigma) = \begin{pmatrix} \cos(\sigma) & \pm i\sin(\sigma) \\ \pm i\sin(\sigma) & \cos(\sigma) \end{pmatrix}\,, \tag{B.0.13}$$

then by setting $c_1 = a_+$, $c_3 = a_-$, $c_2 = b_+$, and $c_4 = b_-$, the positive and negative frequency solutions are

$$\begin{pmatrix} x_\pm^{(0)}(t,\sigma) \\ y_\pm^{(0)}(t,\sigma) \end{pmatrix} = \mathbf{R}_\pm(\sigma)\begin{pmatrix} a_\pm \\ b_\pm \end{pmatrix} e^{\pm it}\,. \tag{B.0.14}$$

This leads to the final form of the solutions as

$$x^{(0)}(t,\sigma) = x_+^{(0)}(t,\sigma) + x_-^{(0)}(t,\sigma)\,, \tag{B.0.15a}$$

Time interval	$t \in [-100, 100]$
Initial conditions	
$y(-100) = 0$	$a_+ = 0.9 - i0.6$
$x(-100) = 1$	$b_+ = -0.2 - i0.4$
$y'(-100) = 0$	$a_- = 0$
$x'(-100) = i$	$b_- = 0$

Table B.1: Initial conditions of the solutions

$$y^{(0)}(t,\sigma) = y_+^{(0)}(t,\sigma) + y_-^{(0)}(t,\sigma)\,. \tag{B.0.15b}$$

In the solution, the slow timescale σ only appears as an angle in the rotation matrix $\mathfrak{R}_\pm(\sigma)$. Further inspection of the slow timescale provides the insight that the expansion parameter appearing in $\sigma = \epsilon^2\tau(t)$ can be absorbed by setting

$$\epsilon^2 h(\epsilon t) = H(t)\,. \tag{B.0.16}$$

This means that the coupled equations Eq. (B.0.1) are now of the form

$$\ddot{x}(t) + x(t) - H(t)y(t) = 0\,,\ \ \ddot{y}(t) + y(t) - H(t)x(t) = 0\,. \tag{B.0.17a}$$

The slow timescale is then rewritten accordingly to

$$\sigma = \epsilon^2\tau(t) = -\frac{1}{2}\int_0^t \epsilon^2 h(\epsilon t')\mathrm{d}t' = -\frac{1}{2}\int_0^t H(t')\mathrm{d}t'\,. \tag{B.0.18}$$

To further illustrate the efficiency of the multiple-scales method, it suffices to compare the analytic result to the exact numerical solution. Therefore, setting $\epsilon = 0.1$ and plotting the real part of $y(t)$, in the region $t \in \{-100, 100\}$, with initial conditions given in Table B.1, there appears to be a nearly perfect overlay of the numerical and analytic solutions (see Fig. B.1).

In Fig. B.2 the difference between the analytic and numerical solution is displayed, where small differences occur mostly at the beginning of the oscillation.

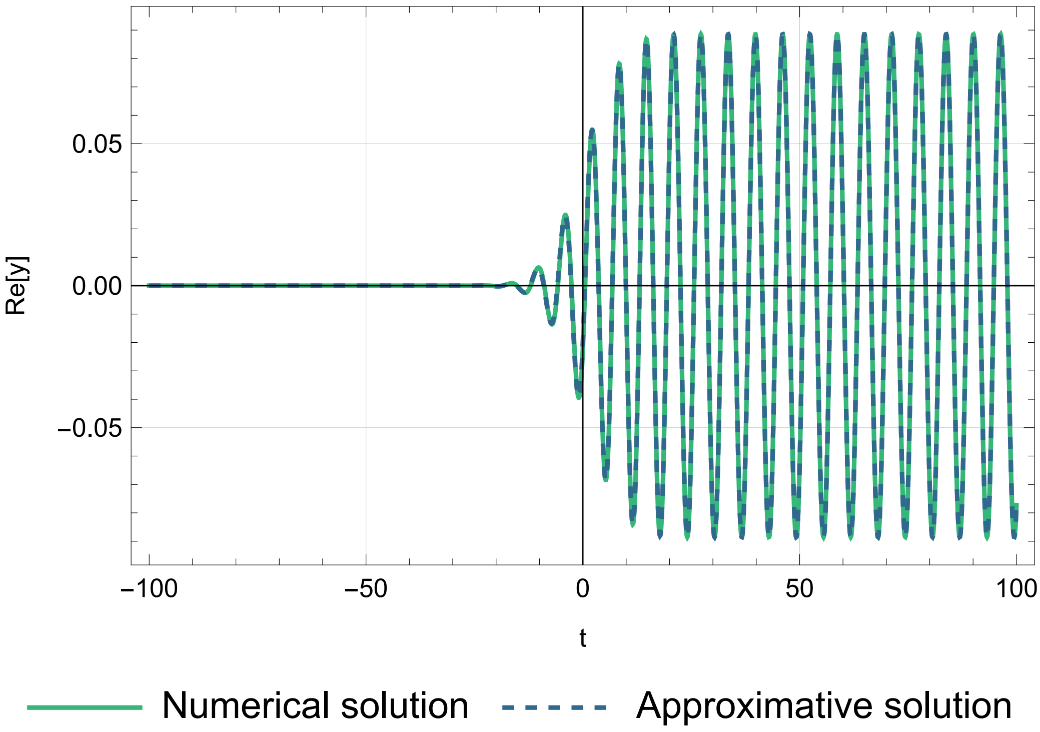

Figure B.1: Comparison of the analytic solution obtained from the multiple-scales method and numerically obtained solutions.

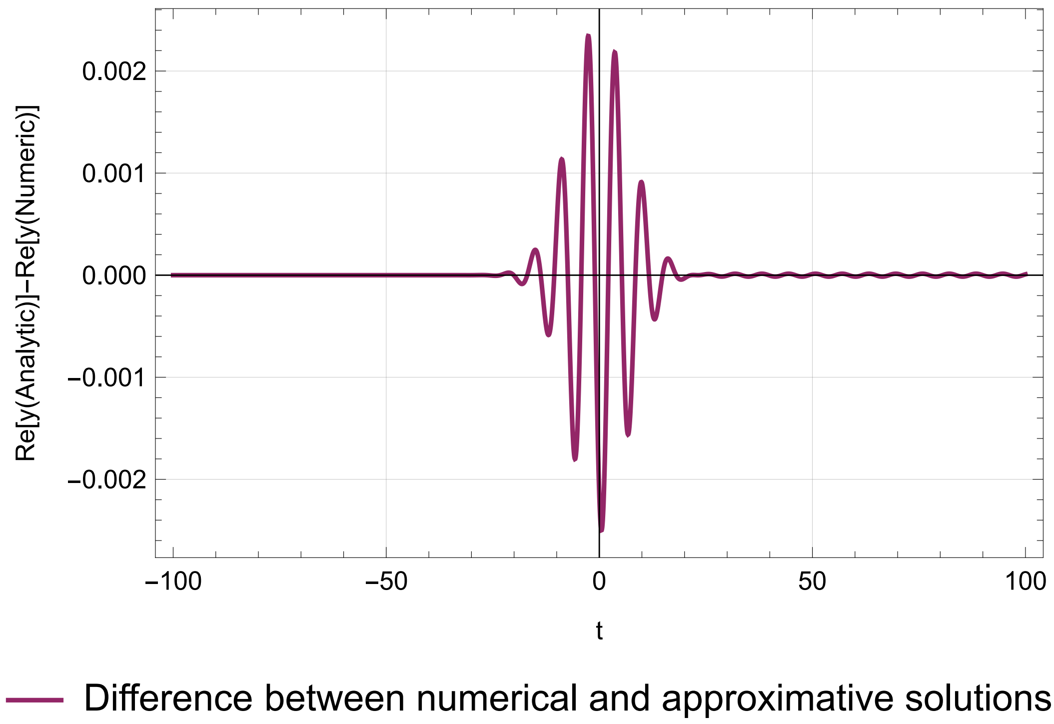

Figure B.2: Difference between the analytic solution obtained from the multiple-scales method and the numerically obtained solution.

Appendix C

Inhomogeneities at $\mathcal{O}(\epsilon^2)$ of the field equations

This section summarizes the second-order inhomogeneities of the field equations given in Eq. (4.2.25). Define the following operators:

$$\mathcal{C}^{\pm}_{(a,b)} = \partial_r \mp \frac{1}{r}\left(a + br^2\beta^2(\varsigma)\right) , \tag{C.0.1}$$

$$\mathcal{K} = r\left(\frac{n^2\omega^2}{\zeta(\varsigma)^2} + \frac{1}{r}\partial_r\right) , \tag{C.0.2}$$

$$\mathcal{L}^{\pm}_{(j,k,l)} = r\left(\frac{n^2\omega^2}{\zeta(\varsigma)^2} \pm \frac{1}{r}\left(j + \frac{1}{r}\frac{\zeta'(\varsigma)^k}{2^l}\partial_r\right)\right) , \tag{C.0.3}$$

$$\mathcal{U} = \zeta'(\varsigma)\beta(\varsigma) + \zeta\beta'(\varsigma) , \tag{C.0.4}$$

$$\mathcal{Z} = i\left(\frac{\zeta'(\varsigma)^2 - \zeta(\varsigma)\zeta''(\varsigma)}{\zeta(\varsigma)} - \zeta'(\varsigma)\partial_r - \zeta(\varsigma)\partial_r^2\right) , \tag{C.0.5}$$

$$\mathcal{V} = \frac{\zeta'(\varsigma)}{r}\partial_r + \frac{\zeta}{r}\partial_r^2 , \tag{C.0.6}$$

$$\mathcal{W} = r\frac{n^2\omega^2}{\zeta(\varsigma)^2} - \frac{1}{r} - \partial_r , \tag{C.0.7}$$

$$\mathcal{Q} = -i\left(\frac{\omega}{\zeta(\varsigma)^2} + \frac{r}{3} + r\partial_r\right) , \tag{C.0.8}$$

$$\mathcal{T}^{\pm} = \frac{n^2r^2\omega^2}{\zeta(\varsigma)^2} \pm 1 \mp r\partial_r . \tag{C.0.9}$$

Then at $\mathcal{O}(\epsilon^2)$, the inhomogeneities are given by

$$\Sigma^0_0 = \frac{1}{3}\sqrt{2}\beta r\left(\bar{R}_{+--s}(\varsigma)a_0^{(0,1)}(r,\varsigma) - \bar{R}_{+-+s}(\varsigma)a_0^{(0,-1)}(r,\varsigma)\right) , \tag{C.0.10a}$$

$$
\begin{aligned}
\Sigma^0_s =& \frac{1}{3}\sqrt{2}\beta r\left(\bar{R}_{+--s}(\varsigma)a_s^{(0,1)}(r,\varsigma)-\bar{R}_{+-+s}(\varsigma)a_s^{(0,-1)}(r,\varsigma)\right)\\
&+ir\left(\bar{R}_{+--s}(\varsigma)C^-_{(2,0)}a_\sharp^{(0,1)}(r,\varsigma)-\bar{R}_{+-+s}(\varsigma)C^-_{(2,0)}a_\flat^{(0,-1)}(r,\varsigma)\right)\\
&-ir\left(\bar{R}_{+--s}(\varsigma)C_{(0,0)}a_\flat^{(0,1)}(r,\varsigma)-\bar{R}_{+-+s}(\varsigma)C_{(0,0)}a_\sharp^{(0,-1)}(r,\varsigma)\right)\,,
\end{aligned}
\tag{C.0.10b}
$$

$$
\begin{aligned}
\Sigma^0_\flat-\bar{R}_{+--s}(\varsigma)\frac{2}{3}\sqrt{2}r\beta a_\flat^{(0,1)}(r,\varsigma) &= -\Sigma^0_\sharp-\bar{R}_{+-+s}(\varsigma)\frac{2}{3}\sqrt{2}r\beta a_\sharp^{(0,-1)}(r,\varsigma)\\
&=\frac{ir}{3}\left(\bar{R}_{+--s}(\varsigma)C^-_{(1,0)}a_s^{(0,1)}(r,\varsigma)+\bar{R}_{+-+s}(\varsigma)C^-_{(1,0)}a_s^{(0,-1)}(r,\varsigma)\right)\,.
\end{aligned}
\tag{C.0.10c}
$$

Next, for $m=\pm1$, the frame components of the inhomogeneities read

$$
\begin{aligned}
\Sigma^{\pm1}_0 =& \,\partial_\varsigma a_0^{(0,\pm1)}(r,\varsigma)\\
&+\frac{ir}{2}\left(\bar{R}_{+s-s}(\varsigma)C^-_{(0,1)}-\frac{1}{6}\bar{R}_{+-+-}(\varsigma)C^-_{(1,0)}\right)a_0^{(0,\pm1)}(r,\varsigma)\\
&+\frac{ir}{4}\bar{R}_{\pm s\pm s}C^-_{(1,1)}a_0^{(0,\mp1)}(r,\varsigma)\\
&+\frac{ir}{2\zeta(\varsigma)}\nabla_+\nabla_-\zeta(\varsigma)\left(\mathcal{K}a_0^{(0,\pm1)}(r,\varsigma)+i\sqrt{2}\omega\left(a_\sharp^{(0,\pm1)}(r,\varsigma)+a_\flat^{(0,\pm1)}(r,\varsigma)\right)\right)\\
&+\frac{ir}{2\zeta(\varsigma)}\nabla_\pm\nabla_\pm\zeta(\varsigma)\left(\mathcal{L}^+_{(1,0,1)}a_0^{(0,\pm1)}(r,\varsigma)-i\sqrt{2}\omega a_{\sharp/\flat}^{(0,\mp1)}(r,\varsigma)\right)\\
&+\frac{ir}{2\zeta(\varsigma)}\left(-\frac{i}{r}\left[\zeta'(\varsigma)\left(\mathcal{U}a_0^{(1,\pm1)}(r,\varsigma)-2\omega a_s^{(1,\pm1)}(r,\varsigma)\right)+\partial_r^2a_0^{(0,\pm1)}(r,\varsigma)\right]\right)\,,
\end{aligned}
\tag{C.0.11a}
$$

$$
\begin{aligned}
\Sigma^{\pm1}_s =& \,\partial_\varsigma a_s^{(0,\pm1)}(r,\varsigma)\\
&-\frac{1}{\sqrt{2}}r\beta\left(\bar{R}_{+s-s}(\varsigma)a_\sharp^{(0,\pm1)}(r,\varsigma)+\bar{R}_{+s-s}(\varsigma)a_\flat^{(0,\pm1)}(r,\varsigma)+\bar{R}_{\pm s\pm s}(\varsigma)a_{\sharp/\flat}^{(0,\mp1)}(r,\varsigma)\right)\\
&-\frac{ir}{2}\left(\frac{1}{3}\bar{R}_{+-+-}(\varsigma)C^-_{(1,0)}+\bar{R}_{+s-s}(\varsigma)C^-_{(0,-1)}\right)a_s^{(0,\pm1)}(r,\varsigma)\\
&-\frac{ir}{4}\bar{R}_{\pm s\pm s}(\varsigma)C^-_{(1,-1)}a_s^{(0,\mp1)}(r,\varsigma)\\
&+\frac{ir}{2\zeta(\varsigma)}\left(\nabla_+\nabla_-\zeta(\varsigma)\mathcal{K}a_s^{(1,\pm1)}(r,\varsigma)+\nabla_\pm\nabla_\pm\zeta(\varsigma)\mathcal{L}^-_{(1,0,0)}a_s^{(0,\pm1)}(r,\varsigma)\right)\\
&+\frac{ir}{2\zeta(\varsigma)}\left(\mathcal{Z}a_s^{(0,\pm1)}(r,\varsigma)+\mathcal{U}a_s^{(1,\pm1)}(r,\varsigma)-\frac{\zeta'(\varsigma)}{\zeta(\varsigma)}\omega n^2a_0^{(1,\pm1)}(r,\varsigma)\right)\,.
\end{aligned}
\tag{C.0.11b}
$$

The following are two equations for Σ, where the plus sign refers to the equation of the first component on the left side of "/", and the minus sign refers to the equation of the component on the right side of "/":

$$\begin{aligned}\Sigma^{\pm1}_{\sharp/\flat} &= \partial_\varsigma a^{(0,\pm1)}_{\sharp/\flat}(r,\varsigma)\\ &+ \frac{ir}{2}\left(\bar{R}_{+s-s}(\varsigma)C^-_{(1,1)}a^{(0,\pm1)}_{\sharp/\flat}(r,\varsigma) + \frac{1}{2}\bar{R}_{\pm s\pm s}(\varsigma)C^-_{(0,1)}a^{(0,\mp1)}_{\sharp/\flat}(r,\varsigma)\right)\\ &- \frac{ir}{6}\bar{R}_{+-+-}(\varsigma)C_{(0,0)}a^{(0,\pm1)}_{\flat/\sharp}(r,\varsigma) + \bar{R}_{+s-s}(\varsigma)\frac{r\beta}{\sqrt{2}}a^{(0,\pm1)}_{s}(r,\varsigma)\\ &+ \frac{ir}{2\zeta(\varsigma)}\left(\nabla_+\nabla_-\zeta(\varsigma)\left(i\frac{n^2\omega}{\zeta^2(\varsigma)}\sqrt{2}a^{(0,\pm1)}_0(r,\varsigma) + \mathcal{Q}a^{(0,\pm1)}_{\sharp/\flat}\right)\right)\\ &+ \frac{ir}{2\zeta(\varsigma)}\left(\nabla_\pm\nabla_\pm\zeta(\varsigma)\mathcal{L}^-_{(0,1,0)}a^{(0,\mp)}_{\sharp/\flat}(r,\varsigma) - \mathcal{V}a^{(0,\pm1)}_{\sharp/\flat}(r,\varsigma)\right),\end{aligned} \tag{C.0.11c}$$

$$\begin{aligned}\Sigma^{\pm1}_{\flat/\sharp} &= \partial_\varsigma a^{(0,\pm1)}_{\flat/\sharp}(r,\varsigma)\\ &+ \frac{r\beta}{\sqrt{2}}\left(\bar{R}_{+s-s}(\varsigma)a^{(0,\pm1)}_{s}(r,\varsigma) + \bar{R}_{\pm s\pm s}(\varsigma)a^{(0,\mp1)}_{s}(r,\varsigma)\right)\\ &+ \frac{ir}{2}\left(\bar{R}_{+s-s}(\varsigma)C^-_{(1,1)}a^{(0,\pm1)}_{\flat/\sharp}(r,\varsigma) + \bar{R}_{\pm s\pm s}(\varsigma)\frac{1}{2}C^-_{(2,1)}a^{(0,\mp1)}_{\flat/\sharp}(r,\varsigma)\right)\\ &- \frac{i}{2}\left(\frac{r}{3}\bar{R}_{+-+-}(\varsigma)C^-_{(2,0)}a^{(0,\pm1)}_{\sharp/\flat}(r,\varsigma) - \bar{R}_{\pm s\pm s}(\varsigma)a^{(0,\mp1)}_{\sharp/\flat}(r,\varsigma)\right)\\ &- \frac{i}{3}\bar{R}_{+-+-}(\varsigma)a^{(0,\pm1)}_{\flat/\sharp}(r,\varsigma) - \frac{ir}{2\zeta(\varsigma)}\mathcal{V}a^{(0,\pm1)}_{\flat/\sharp}\\ &+ \frac{ir}{2\zeta(\varsigma)}\nabla_\pm\nabla_\pm\zeta(\varsigma)\left(\mathcal{W}a^{(0,\mp1)}_{\flat/\sharp}(r,\varsigma) - \frac{1}{2}a^{(0,\mp1)}_{\sharp/\flat}(r,\varsigma) + i\sqrt{2}n^2\omega a^{(0,\mp1)}_0(r,\varsigma)\right)\\ &+ \frac{ir}{2\zeta(\varsigma)}\nabla_+\nabla_-\zeta(\varsigma)\left(\mathcal{W}a^{(0,\pm1)}_{\flat/\sharp}(r,\varsigma) + i\sqrt{2}\omega n^2 a^{(0,\mp1)}_0(r,\varsigma)\right).\end{aligned} \tag{C.0.11d}$$

For $m = \pm2$, the frame components of the inhomogeneities read

$$\Sigma^{\pm2}_0 = \pm r\sqrt{2}\bar{R}_{+-\pm s}(\varsigma)a^{(0,\pm1)}_0(r,\varsigma)\,, \tag{C.0.12a}$$

$$\begin{aligned}\Sigma^{\pm2}_s &= \frac{i}{\beta(\varsigma)}R_{+-\pm s}(\varsigma)\left(\left(2\pm\partial_r\right)a^{(0,\pm1)}_\sharp(r,\varsigma) \mp \partial_r a^{(0,\pm1)}_\flat(r,\varsigma)\right)\\ &+ \frac{1}{\beta(\varsigma)}R_{+-\pm s}(\varsigma)r\sqrt{2}\beta(\varsigma)a^{(0,\pm1)}_s(r,\varsigma)\,,\end{aligned} \tag{C.0.12b}$$

$$\Sigma^{\pm2}_{\sharp/\flat} = \pm\frac{i}{3\beta(\varsigma)}R_{+-\pm s}(\varsigma)\left(\left(1-r\partial_r\right)a^{(0,\pm1)}_s(r,\varsigma) - 2i\sqrt{2}r\beta(\varsigma)a^{(0,\pm1)}_{\sharp/\flat}(r,\varsigma)\right), \tag{C.0.12c}$$

$$\Sigma^{\pm2}_{\flat/\sharp} = \mp\frac{i}{3\beta(\varsigma)}R_{+-\pm s}(\varsigma)\left(\left(5-r\partial_r a^{(0,\pm1)}_s(r,\varsigma)\right) + 4\sqrt{2}r\beta(\varsigma)a^{(0,\pm1)}_{\flat/\sharp}(r,\varsigma)\right). \tag{C.0.12d}$$

Lastly, for $m = \pm 3$, the frame components of the inhomogeneities are given by

$$\begin{aligned}\Sigma_0^{\pm 3} = &\frac{i}{4\beta(\varsigma)} R_{\pm s \pm s}(\varsigma) r \mathcal{C}^{+}_{1,1} a_0^{(0,\pm 1)}(r,\varsigma) + \frac{1}{2\beta(\varsigma)\zeta(\varsigma)} \nabla_\pm \nabla_\pm \zeta(\varsigma) \mathcal{T}^- a_0^{(0,\pm 1)}(r,\varsigma) \\ &+ \frac{1}{2\beta(\varsigma)\zeta(\varsigma)} \nabla_\pm \nabla_\pm \zeta(\varsigma) 2ir^2\sqrt{2}\omega a_{\sharp/\flat}^{(0,\pm 1)}(r,\varsigma)\,,\end{aligned} \tag{C.0.13a}$$

$$\begin{aligned}\Sigma_s^{\pm 3} = &\frac{i}{4\beta(\varsigma)} R_{\pm s \pm s}(\varsigma) \left(\mathcal{C}^{-}_{(1,1)} a_s^{(0,\pm 1)}(r,\varsigma) + 2i\sqrt{2} r \beta(\varsigma) a_{\sharp/\flat}^{(0,\pm 1)}(r,\varsigma) \right) \\ &+ \frac{1}{2\beta(\varsigma)\zeta(\varsigma)} \nabla_\pm \nabla_\pm \zeta(\varsigma) \mathcal{T}^+ a_s^{(0,\pm 1)}(r,\varsigma)\,,\end{aligned} \tag{C.0.13b}$$

$$\begin{aligned}\Sigma_{\sharp/\flat}^{\pm 3} = &\frac{i}{4\beta(\varsigma)} R_{\pm s \pm s}(\varsigma) \mathcal{C}^{-}_{(-2,1)} a_{\sharp/\flat}^{(0,\pm 1)}(r,\varsigma) \\ &+ \frac{1}{2\beta(\varsigma)\zeta(\varsigma)} \nabla_\pm \nabla_\pm \zeta(\varsigma) \mathcal{T}^- a_{\sharp/\flat}^{(0,\pm 1)}(r,\varsigma)\,,\end{aligned} \tag{C.0.13c}$$

$$\begin{aligned}\Sigma_{\flat/\sharp}^{\pm 3} = &\frac{i}{4\beta(\varsigma)} R_{\pm s \pm s}(\varsigma) \left(2i a_{\sharp/\flat}^{(0,\pm 1)}(r,\varsigma) 2r\sqrt{2}\beta(\varsigma) a_s^{(0,\pm 1)}(r,\varsigma) + i\mathcal{C}^{-}_{(0,1)} a_{\flat/\sharp}^{(0,\pm 1)}(r,\varsigma) \right) \\ &+ \frac{1}{2\beta(\varsigma)\zeta(\varsigma)} \nabla_\pm \nabla_\pm \zeta(\varsigma) \left(\frac{ir\omega n^2}{\zeta^2} a_0^{(0,\pm 1)}(r,\varsigma) + \zeta(\varsigma)^{-2} \left(r\omega - ir\partial_r \right) a_{\flat/\sharp}^{(0,\pm 1)}(r,\varsigma) \right) \\ &- \frac{i}{\beta(\varsigma)\zeta(\varsigma)^3} \nabla_\pm \nabla_\pm \zeta(\varsigma) a_{\sharp/\flat}^{(0,\pm 1)}(r,\varsigma)\,.\end{aligned} \tag{C.0.13d}$$

Appendix D

Supplementary material

This chapter contains short derivations and additional material to the main chapters of this thesis.

D.1 Geodesic deviation computation

The full computation of the geodesic deviation equation of Eq. (2.3.11) reads

$$
\begin{aligned}
(\bar{D}_\lambda \bar{D}_\lambda z)^\mu =& \partial_\lambda (\bar{D}_\lambda z)^\mu + \bar{\Gamma}^\mu_{\alpha\beta} m^\alpha (\bar{D}_\lambda z)^\beta \\
=& \partial_\lambda (\partial_\lambda z^\mu + \bar{\Gamma}^\mu_{\alpha\beta} m^\alpha z^\beta) + \bar{\Gamma}^\mu_{\alpha\beta} m^\alpha (\partial_\lambda z^\beta + \bar{\Gamma}^\beta_{\rho\delta} m^\rho z^\delta) \\
=& \partial_\lambda \bar{\Gamma}^\mu_{\alpha\beta} m^\alpha z^\beta + \bar{\Gamma}^\mu_{\alpha\beta} m^\alpha \partial_\lambda z^\beta + \bar{\Gamma}^\mu_{\alpha\beta} m^\alpha \partial_\lambda z^\beta + \bar{\Gamma}^\mu_{\alpha\beta} m^\alpha \bar{\Gamma}^\beta_{\rho\delta} m^\rho z^\delta \\
=& \partial_\lambda \bar{\Gamma}^\mu_{\alpha\beta} m^\alpha z^\beta + 2\bar{\Gamma}^\mu_{\alpha\beta} m^\alpha \partial_\lambda z^\beta + \bar{\Gamma}^\mu_{\alpha\beta} m^\alpha \bar{\Gamma}^\beta_{\rho\delta} m^\rho z^\delta \\
=& \bar{\Gamma}^\mu_{\alpha\beta,\gamma} m^\alpha m^\gamma (\lambda \eta^\beta_\perp + \eta^\beta_\parallel) + 2\bar{\Gamma}^\mu_{\alpha\beta} m^\alpha \eta^\beta_\perp + \bar{\Gamma}^\mu_{\alpha\beta} \bar{\Gamma}^\beta_{\rho\delta} m^\alpha m^\rho (\lambda \eta^\delta_\perp + \eta^\delta_\parallel) \\
=& \bar{\Gamma}^\mu_{\alpha\beta,\gamma} m^\alpha m^\gamma \eta^\beta_\parallel + 2\bar{\Gamma}^\mu_{\alpha\beta} m^\alpha \eta^\beta_\perp + \bar{\Gamma}^\mu_{\alpha\beta} \bar{\Gamma}^\beta_{\rho\delta} m^\alpha m^\rho \eta^\delta_\parallel \\
& + \lambda (\bar{\Gamma}^\mu_{\alpha\beta,\gamma} m^\alpha m^\gamma \eta^\beta_\perp + \bar{\Gamma}^\mu_{\alpha\beta} \bar{\Gamma}^\beta_{\rho\delta} m^\alpha m^\rho \eta^\delta_\perp) \\
=& \bar{\Gamma}^\mu_{\alpha\beta,\gamma} m^\alpha m^\gamma \eta^\beta_\parallel + 2\bar{\Gamma}^\mu_{\alpha\beta} m^\alpha \eta^\beta_\perp + \bar{\Gamma}^\mu_{\alpha\beta} \bar{\Gamma}^\beta_{\rho\delta} m^\alpha m^\rho \eta^\delta_\parallel \\
& + \lambda (\bar{\Gamma}^\mu_{\alpha\beta,\gamma} m^\alpha m^\gamma \eta^\beta_\perp + \bar{\Gamma}^\mu_{\alpha\beta} \bar{\Gamma}^\beta_{\rho\delta} m^\alpha m^\rho \eta^\delta_\perp) \,.
\end{aligned}
\tag{D.1.1}
$$

D.2 Derivation of the impedance relation

In the following, the relation between the two volume forms ϵ and $\tilde{\epsilon}$, given in Eq. (2.4.9), is derived. To begin with, note that the metric transforms under a change of coordinates as

$$
g' = (J^{-1})^T g \, J^{-1} \,, \tag{D.2.1}
$$

where J is the Jacobi matrix. Applying the determinant and taking the square root amounts to

$$
\sqrt{-\det g'} = (\det J)^{-1} \sqrt{-\det g} \,. \tag{D.2.2}
$$

Since g and $\bar{g}$ transform according to Eq. (D.2.1) respectively, their ratio

$$\frac{\sqrt{-\det g'}}{\sqrt{-\det \bar{g}'}} = \frac{\sqrt{-\det g}}{\sqrt{-\det \bar{g}}}\,, \tag{D.2.3}$$

forms an invariant. The invariance of the ratio allows for an evaluation in the rest frame via

$$\frac{\sqrt{-\det g}}{\sqrt{-\det \bar{g}}} = n\,, \tag{D.2.4}$$

where n is the refractive index defined in Eq. (2.4.7). In terms of the optical metric Eq. (D.2.4) reads

$$\frac{\sqrt{-\det g}}{\sqrt{-\det \tilde{g}}} = \frac{n}{\mu} = \frac{1}{\eta}\,, \tag{D.2.5}$$

where η denotes the wave impedance.

D.3 Motivation for the scale-dependence of the spatial Riemann curvature tensor

To motivate Eq. (4.1.2), consider a Newtonian $\frac{1}{r}$-potential of the form

$$\phi = -\frac{\mathrm{M}}{r}\,, \tag{D.3.1}$$

for some mass parameter M. Placing a straight optical fiber with length s vertically in this potential, the radius changes according to $r = L + s$, hence

$$\phi = -\frac{\mathrm{M}}{(L+s)}\,, \tag{D.3.2}$$

with $L > 2\mathrm{M}$ and $s \ll L$. The Riemann curvature tensor is related to the second derivatives of the potential

$$\phi'' = 2\mathrm{M}r^{-3}\,. \tag{D.3.3}$$

Therefore, the potential given in Eq. (D.3.2) gives rise to

$$R \sim \frac{2\mathrm{M}}{L^3}\left(1+\frac{s}{L}\right)^{-3} \approx \frac{2M}{L^3}\left(1-\frac{3s}{L}\right)\,. \tag{D.3.4}$$

A relation of the form given in Eq. (4.1.1) is now obtained by either choosing a new length scale, e.g. setting $L = l_b$ for which $l_0/L = \tilde{\varepsilon} \ll 1$ is satisfied, or by considering the following. Restrict the potential to Earth's gravitational field and fix $L = R_\oplus$ to Earth's radius and mass $\mathrm{M} = \mathrm{M}_\oplus$, respectively. Hence, by choosing the core radius l_0 as the characteristic length scale, the Riemann tensor may be expressed via second derivatives of ϕ as

$$R_{sijs} \sim \varepsilon^2 \partial_i \partial_j \phi \left(\frac{\varepsilon s}{l_0} \right) , \tag{D.3.5}$$

which thus motivates the relation provided in Eq. (4.1.2).

D.4 Gauge function w.r.t. the optical metric

The aim of this section is to express the gauge function given in Eq. (2.4.13), in terms of the optical covariant derivative by expanding the divergence and using Eq. (2.4.10):

$$\begin{aligned}
\chi &= \frac{1}{\sqrt{\mu}} \nabla_a \left(\sqrt{\mu} \tilde{g}^{ab} A_b \right) && \text{(D.4.1)}\\
&= \frac{1}{\sqrt{\mu}} \frac{1}{\sqrt{-\det g}} \partial_a \left(\sqrt{\mu} \sqrt{-\det g}\, \tilde{g}^{ab} A_b \right) && \text{(D.4.2)}\\
&= \frac{1}{\sqrt{\mu}} \eta \frac{1}{\sqrt{-\det \tilde{g}}} \partial_a \left(\sqrt{\mu} \eta \sqrt{-\det \tilde{g}}\, \tilde{g}^{ab} A_b \right) && \text{(D.4.3)}\\
&= \frac{1}{\sqrt{\epsilon}} \frac{1}{\sqrt{-\det \tilde{g}}} \partial_a \left(\sqrt{\epsilon} \sqrt{-\det \tilde{g}}\, \tilde{g}^{ab} A_b \right) && \text{(D.4.4)}\\
&= \frac{1}{\sqrt{\epsilon}} \tilde{\nabla}_a \left(\sqrt{\epsilon} \tilde{g}^{ab} A_b \right) . && \text{(D.4.5)}
\end{aligned}$$

Bibliography

[1] J. Ballato and P. Dragic. “Glass: the carrier of light-a brief history of optical fiber”. In: *International Journal of Applied Glass Science* 7.4 (2016), pp. 413–422.

[2] D. Colladon. “On the reflections of a ray of light inside a parabolic liquid stream”. In: *Comptes Rendus* 15.800-802 (1842), p. 15.

[3] J. Babinet. “Note on the transmission of light by sinuous canals”. In: *Comptes Rendus* 15 (1842), p. 802.

[4] P. M. Heimann. “Maxwell, Hertz, and the nature of electricity”. In: *Isis* 62.2 (1971), pp. 149–157.

[5] A. G. Bell. “The photophone”. In: *Science* 11 (1880), pp. 130–134.

[6] A. G. Bell. “The Invention of the Telephone”. In: *Electrical Review and Western Electrician* 59.20 (Nov. 1911), pp. 130–134.

[7] A. L. von Reuss. *Vorläufige Mittheilung über Durchleuchtung der Augenwandungen*. Wiener klinische Wochenschrift - the central European journal of medicine, Springer-Verlag GmbH, Wien, Austria, 1888. URL: `http://anno.onb.ac.at/cgi-content/anno?aid=wkw`.

[8] M. El-Gomati, M. D. Al-Amri, and M. Suhail Zubairy. *Optics in Our Time*. eng. 1st ed. 2016. Cham: Springer Open, 2016. ISBN: 9789811015595.

[9] P. D. Dragic and J. Ballato. “120 Years of Optical Glass Science”. In: *Optics & Photonics News* 25.5 (May 2014), p. 44. DOI: `10.1364/OPN.25.5.000044`.

[10] *The Nobel Prize in Physics*. 2009. URL: `http://nobelprize.org/nobel_prizes/physics/laureates/2009/index.html`.

[11] D. K. F. Kapron and R. Maurer. “Radiation Losses in Glass Optical Waveguides”. In: *Appl. Phys. Lett.* 17.423–425 (1970).

[12] Y. Kang et al. “Measurement of the Entanglement between Photonic Spatial Modes in Optical Fibers”. In: Phys. Rev. Lett. 109.2, 020502 (July 2012), p. 020502. DOI: `10.1103/PhysRevLett.109.020502`.

[13] J. M. Thomas et al. “Quantum Teleportation Coexisting with Conventional Classical Communications in Optical Fiber”. In: *arXiv e-prints*, arXiv:2404.10738 (Apr. 2024), arXiv:2404.10738. DOI: `10.48550/arXiv.2404.10738`. arXiv: `2404.10738 [quant-ph]`.

[14] Z. Pan et al. “Measurement of gravitational lensing of the cosmic microwave background using SPT-3G 2018 data”. In: Phys. Rev. D 108.12, 122005 (Dec. 2023), p. 122005. DOI: 10.1103/PhysRevD.108.122005. arXiv: 2308.11608 [astro-ph.CO].

[15] S. Manly and E. Page. “Experimental feasibility of measuring the gravitational redshift of light using dispersion in optical fibers”. In: Phys. Rev. D 63.6, 062003 (Mar. 2001), p. 062003. DOI: 10.1103/PhysRevD.63.062003. arXiv: gr-qc/0008004 [gr-qc].

[16] *Gravitational interferometry with entangled states in optical fibers.* 2023. DOI: 10.3030/101071779. URL: https://cordis.europa.eu/project/id/101071779/de.

[17] T. B. Mieling. “Gupta–Bleuler Quantization of the Electromagnetic Field in Curved Space-Times with Applications to Gravitational Photon Interferometry”. Doctoral thesis. University of Vienna, 2023.

[18] S. M. Rytov. “On the transition from wave to geometrical optics”. In: *Doklady Akademii Nauk SSSR* 263.28 (1938).

[19] V. V. Vladimirskii. “On the rotation of the plane of polarization in a curved light ray”. In: *Doklady Akademii Nauk SSSR* 222.31 (1941).

[20] T. B. Mieling and M. A. Oancea. “Polarization transport in optical fibers beyond Rytov’s law”. In: *Physical Review Research* 5.2, 023140 (May 2023), p. 023140. DOI: 10.1103/PhysRevResearch.5.023140. arXiv: 2302.10540 [physics.optics].

[21] B. Markovski and S. I. Vinitsky, eds. *Topological phases in quantum theory. International Seminar on Geometrical Aspects of Quantum Theory. Dubna, USSR, 2-4 September 1988.* eng. Singapore: World Scientific, 1989. ISBN: 9971-50-877-X.

[22] M.-Y. Lai et al. “Electromagnetic wave propagating along a space curve”. In: *Phys. Rev. A* 97 (3 Mar. 2018), p. 033843. DOI: 10.1103/PhysRevA.97.033843. URL: https://link.aps.org/doi/10.1103/PhysRevA.97.033843.

[23] R. Nityananda and S. Sridhar. “Light beams with general direction and polarization: Global description and geometric phase”. In: *Annals of Physics* 341 (2014), pp. 117–131. ISSN: 0003-4916. DOI: 10.1016/j.aop.2013.11.010. URL: https://www.sciencedirect.com/science/article/pii/S0003491613002716.

[24] E. Fermi. “Sopra i fenomeni che avvengono in vicinanza di una linea oraria”. In: *Rend. Lincei* 31 (1922), pp. 21–23.

[25] A. G. Walker. “XXI.—Relative Co-ordinates”. In: *Proceedings of the Royal Society of Edinburgh* 52 (1933), pp. 345–353. DOI: 10.1017/S0370164600019611.

[26] D. Bini and R. T. Jantzen. *Circular Holonomy, Clock Effects and Gravitoelectromagnetism: Still Going Around in Circles After All These Years.* 2002. arXiv: gr-qc/0202085 [gr-qc].

[27] E. Bortolotti. "Sulle rappresentazioni conformi, e su di una interpretazione fisica del parallelismo di Levi-Civita". In: *Atti della Reale Accademia Nazionale dei Lincei.* 6th ser. 4 (1926), pp. 552–526.

[28] M. Spivak. *A Comprehensive Introduction to Differential Geometry.* A Comprehensive Introduction to Differential Geometry Bd. 1. Publish or Perish, Incorporated, 1999. ISBN: 9780914098706. URL: https://books.google.at/books?id=ahSWQgAACAAJ.

[29] R. C. Jones. "A New Calculus for the Treatment of Optical SystemsI. Description and Discussion of the Calculus". In: *J. Opt. Soc. Am.* 31.7 (July 1941), pp. 488–493. DOI: 10.1364/JOSA.31.000488. URL: https://opg.optica.org/abstract.cfm?URI=josa-31-7-488.

[30] L. Landau and Lifshitz. *Electrodynamics of Continuous Media.* Ed. by M. Robert Maxwell. Vol. 8. Course of Theoretical Physics. Pergamon Press, 1984, p. 292.

[31] S. I. Vinitskiĭ et al. "Reviews of topological problems: Topological phases in quantum mechanics and polarization optics". In: *Soviet Physics Uspekhi* 33.6 (June 1990), pp. 403–428. DOI: 10.1070/PU1990v033n06ABEH002598.

[32] D. Banerjee. "The spinorial representation of polarized light and Berry phase". In: *arXiv e-prints*, arXiv:1107.1868 (July 2011), arXiv:1107.1868. DOI: 10.48550/arXiv.1107.1868. arXiv: 1107.1868 [physics.optics].

[33] N. R. Sadykov. "Rytov-Vladimirsky polarization effect". In: *Optics and Spectroscopy* 92.4 (Apr. 2002), pp. 584–587. DOI: 10.1134/1.1473600.

[34] J. N. Ross. "The rotation of the polarization in low birefringence monomode optical fibres due to geometric effects". In: *Optical and Quantum Electronics* 16 (Sept. 1984), pp. 455–461. ISSN: 0306-8919.

[35] A. Tomita and R. Y. Chiao. "Observation of Berry's topological phase by use of an optical fiber". In: *Physical review letters* 57.8 (1986), p. 937.

[36] P. Sonawala. "Rotation of polarization in single mode optical fibers and its relation to Berry's Phase". MSc thesis. Oregon State University, 1988. URL: https://ir.library.oregonstate.edu/concern/graduate_thesis_or_dissertations/9g54xn458.

[37] J. Anders. "Evolution of polarization along a single mode fiber". MSc thesis. Oregon State University, 1988. URL: https://ir.library.oregonstate.edu/concern/graduate_thesis_or_dissertations/9g54xn458.

[38] M. V. Berry. "Interpreting the anholonomy of coiled light". In: *Nature* 326.6110 (1987), pp. 277–278. DOI: 10.1038/326277a0. URL: https://doi.org/10.1038/326277a0.

[39] M.-Y. Lai et al. “Geometrical phase and Hall effect associated with the transverse spin of light”. In: Phys. Rev. A 100.3, 033825 (Sept. 2019), p. 033825. DOI: 10.1103/PhysRevA.100.033825.

[40] J. M. Lee. *Introduction to smooth manifolds.* eng. 2. ed. Graduate texts in mathematics 218. New York, NY: Springer, 2013. ISBN: 9781441999818.

[41] B. O’Neill. *Semi-Riemannian geometry : with applications to relativity.* eng. 4. print. Pure and applied mathematics 103. Orlando: Acad. Pr., 1993. ISBN: 0125267401.

[42] H. Ringström. *The Cauchy problem in general relativity.* eng. Vol. 6. European Mathematical Society, 2009. ISBN: 3037195533.

[43] E. Gourgoulhon. *3+1 Formalism in General Relativity: Bases of Numerical Relativity.* eng. c2012. Vol. 846. Lecture Notes in Physics. Berlin, Heidelberg: Springer Nature, 2012. ISBN: 9783642245251.

[44] R. Arnowitt, S. Deser, and C. W. Misner. “Dynamical structure and definition of energy in general relativity”. In: *Physical Review* 116.5 (1959), p. 1322.

[45] D. Chruściński. *Geometric phases in classical and quantum mechanics.* eng. Vol. 36. Progress in mathematical physics. Boston, Mass.: Birkhäuser, 2004. ISBN: 081764282X.

[46] L. Ó. Raifeartaigh. “Fermi Coordinates”. In: *Proceedings of the Royal Irish Academy. Section A: Mathematical and Physical Sciences* 59 (1957), pp. 15–24. ISSN: 00358975. URL: http://www.jstor.org/stable/20520650 (visited on 06/18/2024).

[47] F. W. Hehl. *Foundations of classical electrodynamics : charge, flux, and metric.* eng. Vol. 33. Progress in mathematical physics. Boston, Mass.: Birkhäuser, 2003. ISBN: 9780817642228.

[48] T. B. Mieling. “Gupta-Bleuler quantization of optical fibers in weak gravitational fields”. In: Phys. Rev. A 106.6, 063511 (Dec. 2022), p. 063511. DOI: 10.1103/PhysRevA.106.063511. arXiv: 2207.13537 [quant-ph].

[49] F. K. Manasse and C. W. Misner. “Fermi Normal Coordinates and Some Basic Concepts in Differential Geometry”. eng. In: *Journal of mathematical physics* 4.6 (1963), pp. 735–745. ISSN: 0022-2488.

[50] D. Bini and R. T. Jantzen. “Circular holonomy, clock effects and gravitoelectromagnetism: Still going around in circles after all these years”. In: *Nuovo Cimento B Serie* 117.911 (Sept. 2002), p. 983. DOI: 10.48550/arXiv.gr-qc/0202085. arXiv: gr-qc/0202085 [gr-qc].

[51] W. Gordon. “Zur Lichtfortpflanzung nach der Relativitätstheorie”. In: *Annalen der Physik* 377.22 (1923), pp. 421–456. ISSN: 0003-3804.

[52] L. Hörmander. *The Analysis of Linear Partial Differential Operators I. Distribution Theory and Fourier Analysis.* Second Edition. Classics in Mathematics. Berlin, DE: Springer, 1990. 440 pp. ISBN: 3-540-52343-X.

[53] J.-M. Liu. *Photonic devices.* eng. New York : Cambridge, 2005. ISBN: 0511081979.

[54] J. E. Gómez-Correa et al. "On the physics of propagating Bessel modes in cylindrical waveguides". In: *American Journal of Physics* 85.5 (May 2017), pp. 341–345. DOI: 10.1119/1.4976698. arXiv: 1612.01959 [physics.optics].

[55] *Corning® SMF-28e+® Optical Fiber.* Corning Optical Communications LLC. URL: https://www.corning.com/media/worldwide/coc/documents/Fiber/PI-1463-AEN.pdf. Retrieved on 23.01.2024.

[56] *Corning® SMF-28e® Photonic Fiber.* Corning Optical Communications LLC. URL: https://www.bismon.com/pdf/SMF-28e%20Bare%20Fiber.pdf. Retrieved on 23.01.2024.

[57] C. M. Bender. *Advanced mathematical methods for scientists and engineers. 1, Asymptotic methods and perturbation theory.* eng. New York, NY: Springer, 1999. ISBN: 9781441931870.

[58] T. B. Mieling, C. Hilweg, and P. Walther. "Measuring space-time curvature using maximally path-entangled quantum states". In: Phys. Rev. A 106.3, L031701 (Sept. 2022), p. L031701. DOI: 10.1103/PhysRevA.106.L031701. arXiv: 2202.12562 [gr-qc].

[59] C. M. Will. *Theory and experiment in gravitational physics.* eng. Rev. ed. Cambridge: Cambridge University Press, 1993. ISBN: 0-511-56424-4.

[60] Q. Exirifard, E. Culf, and E. Karimi. "Towards communication in a curved spacetime geometry". In: *Communications Physics* 4.1, 171 (Dec. 2021), p. 171. DOI: 10.1038/s42005-021-00671-8. arXiv: 2009.04217 [gr-qc].

[61] G. P. Agrawal. *Fiber-Optic Communication Systems.* eng. 4th ed. Wiley Series in Microwave and Optical Engineering Ser. ; v.222. See chapter 7 for details on maximum transmission distance. Hoboken : John Wiley and Sons, Incorporated, 2010. ISBN: 9780470918517.

[62] J. Bürger et al. "Impact of coordinate frames on mode formation in twisted waveguides". In: Phys. Rev. B 109.16, 165301 (Apr. 2024), p. 165301. DOI: 10.1103/PhysRevB.109.165301. arXiv: 2311.15770 [physics.optics].

[63] A. Papp and H. Harms. "Polarization optics of liquid-core optical fibers". In: Appl. Opt. 16.5 (May 1977), pp. 1315–1319. DOI: 10.1364/AO.16.001315.

[64] W. F. Yeung and A. R. Johnston. "Effect of temperature on optical fiber transmission". In: Appl. Opt. 17.23 (Dec. 1978), pp. 3703–3705. DOI: 10.1364/AO.17.003703.

[65] M. Kovacevic and A. Djordjevich. "Temperature Dependence Analysis of Mode Dispersion in Step Index Polymer Optical Fibers". In: *Acta Physica Polonica A* 116.4 (Oct. 2009), p. 649. DOI: 10.12693/APhysPolA.116.649.

[66] R. M. Wald. *General relativity.* eng. Chicago: Univ. of Chicago Press, 1984. ISBN: 0226870332.